Chapter 3

Radiation

Lead Authors: Victor I. Fomichev & Piers M. Forster

Co-authors: Chiara Cagnazzo, Andreas I. Jonsson, Ulrike Langematz, Eugene Rozanov, Victoria Falaleeva, Boris Fomin, Nathan Gillett, Michael Iacono, Alexey Karpechko, Jiangnan Li, Perrine Lemennais, Bernard Mayer, Eli Mlawer, Olaf Morgenstern, Gunnar Myhre, Sophie Oberländer, Robert Portmann, Michael Sigmond

3.1 Introduction

Understanding and quantifying radiative processes is of fundamental importance to the study of climate and its change. Radiative processes drive global climate change and play a key role in establishing the temperature structure of the atmosphere. The thermal regime of the middle atmosphere is determined to a great extent by the balance between the incoming solar and outgoing infrared radiation. The radiative heating changes brought on by changes in carbon dioxide and ozone can cause large trends in stratospheric temperatures as well as affect surface climate (WMO, 2003). Given the prime importance of radiative processes for understanding the atmosphere and its evolution, the development and improvement of radiation schemes is obviously one of the crucial points in the ongoing development and maintenance of atmospheric models. The purpose of this chapter is to evaluate key radiative processes in the CCMVal models.

This chapter covers a number of topics. Current radiative parameterisation architecture is assessed in Section 3.2. Global mean temperature profiles and long-term trends provided by CCMVal models are analysed in Section 3.3. In Section 3.4, radiative transfer schemes of different CCMVal models are compared with each other and compared against line-by-line (LBL) calculations. The

incoming solar irradiance at short wavelengths significantly varies with the solar cycle, leading to strong ozone and temperature solar signals in the stratospheric climate. The ability of CCMval models' radiation schemes to reproduce the solar signal is analysed in Section 3.5. The last Section 3.6 presents metric summaries, model by model analysis and a brief overall summary of the chapter.

3.1.1 Radiative based diagnostics

Table 3.1 presents the details of the radiative diagnostics and the metrics used to assess them.

Throughout the chapter we have tried to explain differences between CCMs. However, in many instances appropriate diagnostics were not available and interpretation is lacking, so a full assessment of differences has not been possible.

Several radiative processes are not assessed in this chapter. A representation of photolysis is of fundamental importance for CCMs: this aspect of radiation is discussed in Chapter 6. Above 70 km, local thermodynamic equilibrium (LTE) begins to breakdown (see Fomichev 2009 for a detailed review of non-LTE effects). At present only two CCMs include these effects (CMAM and WACCM), and both employ the same parameterisation (Fomichev *et al*., 1998; Ogibalov and Fomichev, 2003). Clouds and aerosols (both stratospheric and tropospheric) also have important effects on stratospheric heating rates and on radiative forcing but these effects are not evaluated here. We also do not assess the effects of the plane parallel atmosphere approximation that is typically employed in radiation codes. This approximation fails to give any solar heating at zenith angles larger than 90°. Lastly, we do not assess the way the radiation scheme is implemented within the CCM. Important considerations here are the frequency of full radiative calculations compared to the model time step; sub-grid-scale variations and the order of the radiation call in relation to the call to other physical parameterisations.

3.2 Radiative Transfer Parameterisation

Accurate methods of solving radiative transfer within the Earth's atmosphere exist. However, such schemes are too computationally expensive to currently be employed within a climate modelling context. Parameterisations were designed to approximate more exact treatments with sufficient enough accuracy for the problem being considered. A good example of this is one of the earliest parameterisations of solar radiative transfer (Lacis and Hansen, 1974). Their approximations provide useful insights into more complex ones used today. Even their simple parameterisation accounted for Rayleigh scattering, cloud, solar zenith angle, water vapour and ozone absorption, but like many shortwave codes today, it ignored minor absorption by CO_2 and CH_4 (see Collins *et al*., 2006). For its purpose the code was extremely accurate and only increased the computer time overhead in the parent model by 0.3%; variants of this code were employed in climate models until very recently. Much of their original paper was concerned with finding measurements of input properties to test their code and they made the point that uncertainties in water vapour or cloud radiative properties are likely to be a bigger source of error than their approximate radiative transfer solution – this still remains true today.

Radiative transfer approximations within climate models encompass three broad categories of 1) the radiative transfer solution, 2) input parameters and 3) implementation. These are described briefly below

1. *Radiative transfer solution*. The most important choice here is the number of spectral bands to employ and how to account for overlapping within bands. Also important are the number of streams used for scattering approximations. In the CCM context it is also worth considering the choice of a plane parallel atmosphere: nearly all climate models including CCMs adopt this approximation, even when the photolysis codes in CCMs adopt spherical geometry. Most CCMs would therefore not have any solar heating at zenith angles greater than 90°, but still have photolysis of ozone in the stratosphere, creating an inconsistency.
2. *Input parameters*. Important choices include line databases and cross-sections for the absorbing gases and the water vapour continuum; the extra-terrestrial solar spectrum; and cloud and aerosol optical properties.
3. *Implementation*. CCMs and climate models also have to make pragmatic choices about how often to call the radiative transfer code, as calling the code every time step is often impractical and unnecessary. Also choices of cloud overlap and sub-grid-scale variability need to be made. Ways of calculating solar zenith angle and Earth-Sun distance can also cause differences between models. Differences in the underlying model's vertical resolution can also affect the radiation scheme.

Several previous inter-comparisons of climate model radiative transfer codes have been undertaken (*e.g*., Forster *et al*., 2001; Collins *et al*., 2006; Goldblatt *et al*., 2009; Myhre *et al*., 2009). Most of these studies have found very significant differences between radiation codes, even when considering only clear skies and constraining many of the input parameters. Common problems identified have been the use of radiation codes beyond their original specification and/or using outdated input data for, for example, spectral line databases.

Table 3.1: Summary of the radiative diagnostics and the metrics used to assess them.

Process	Diagnostic	Variables	Data	Metric	Section
Stratospheric temperatures	Comparing 1980-1999 climatological global mean temperature profiles	Temperature, Atmospheric composition	(Re)analyses	Maximum difference between ERA-40 and either UKMO or NCEP analysis	3.3
Stratospheric temperature change	Comparing 1980-1999 global mean temperature trends	Temperature, Atmospheric composition	MSU/SSU trends	MSU/SSU trend uncertainty 95% confidence interval	3.3
Radiative fluxes	Comparing climatological fluxes in offline radiation schemes	Shortwave, longwave up/down/ net fluxes for global diurnal average	LBL and other sophisticated offline radiation models	Maximum difference between sophisticated radiation models	3.4
Radiative forcing	Comparing forcings in offline radiation schemes for a variety of atmospheric composition changes	Global and diurnal mean shortwave, longwave up/down/ net instantaneous forcings.	LBL and other sophisticated offline radiation models	Maximum difference between sophisticated radiation models	3.4
Stratospheric heating/ cooling	Comparing climatological heating/ cooling rates in offline radiation schemes	Global and diurnal mean shortwave, longwave, net heating rates	LBL and other sophisticated offline radiation models	Maximum difference between sophisticated radiation models	3.4
Changes in stratospheric heating/ cooling	Comparing changes in heating/cooling rates in offline radiation schemes	Global and diurnal mean changes in shortwave, longwave, net heating rates	LBL and other sophisticated offline radiation models	Maximum difference between sophisticated radiation models	3.4
Solar variability	Comparing SW heating rates in offline radiation schemes with prescribed solar spectrum variations and ozone change	Shortwave heating rates	Sophisticated offline radiation model	Whether or not radiation code reproduces sophisticated model signal	3.5

Some details of the CCM radiation codes employed are presented in Chapter 2 Tables 2.10 and 2.11. All employ versions of the two stream approximation for solving scattering and have an order of 10 spectral bands in the shortwave and longwave. Although all codes include the main absorbers, minor absorbers differ between codes. They also employ different spectral line databases.

3.3 Global mean temperature and temperature trends in CCMs

In this section the performance of the models in terms of their global mean temperature climatology and global mean temperature trends is assessed. On a globally averaged basis the temperature in the middle atmosphere below about 70 km is controlled mainly by radiative processes. This means that long-term global mean temperature biases between models and observations are mainly due to either inaccuracies in the model treatments of radiative processes or due to inaccurate distributions of radiatively active gases in the models. Below 70 km the major contributions to the radiative energy budget are provided by ozone, carbon dioxide, and water vapour. For CCMVal, carbon dioxide is specified identically in all models so its abundance should not contribute to any model differences. However, the distributions of ozone and water vapour, which are affected by the transport and chemistry schemes of each individual model, affect the calculated temperature biases. Overestimation of ozone should generally lead to a

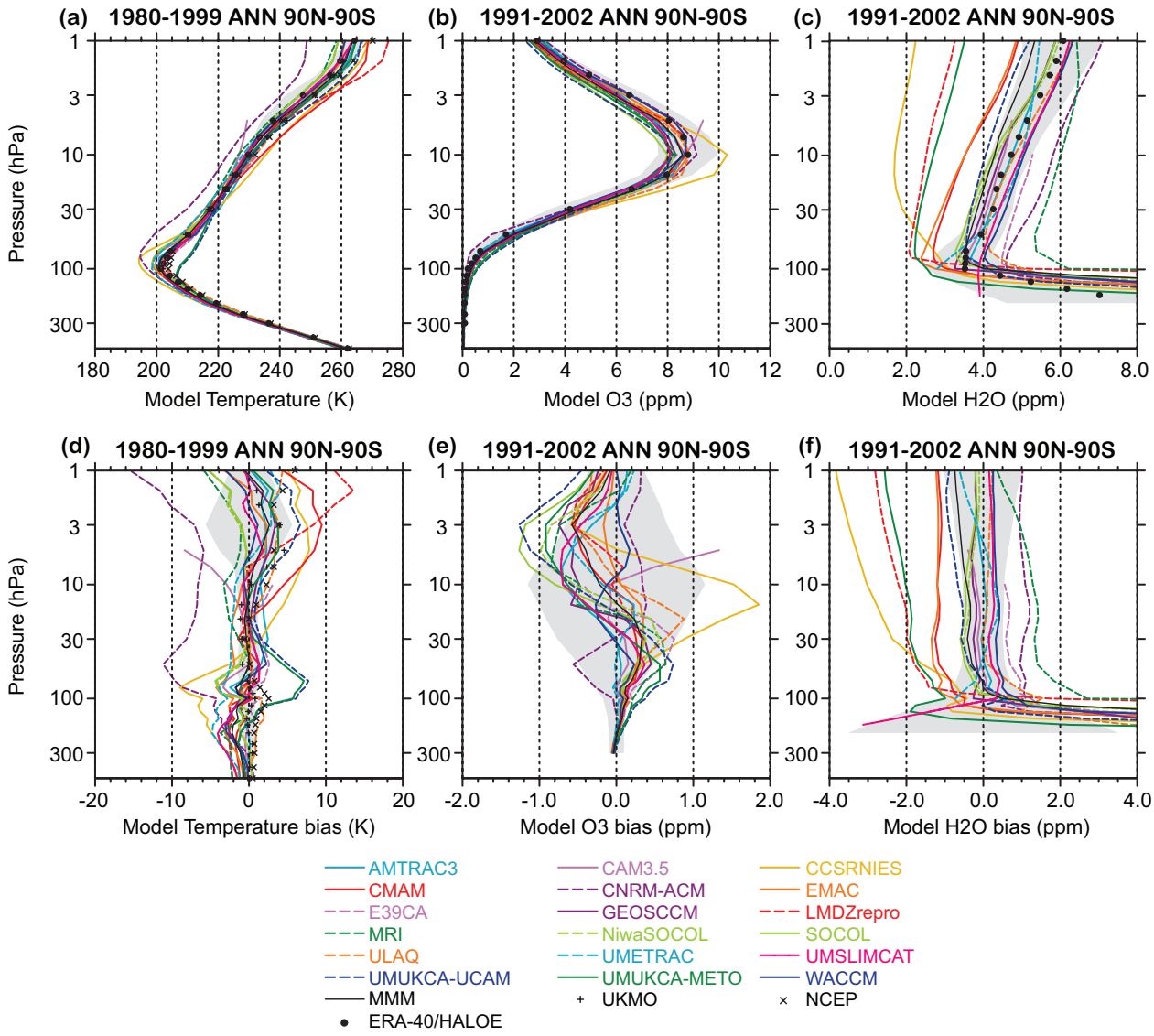

Figure 3.1: Climatological global and annual mean (a) temperature, (b) ozone mixing ratio, and (c) water vapour mixing ratio for REF-B1 model simulations and reference data sets; and (d) temperature bias, (e) ozone bias and (f) water vapour bias with respect to reference data sets. Reference data sets include ERA-40, NCEP and UKMO reanalyses for temperature and HALOE observations for ozone and water vapour. For temperature, the climatological means and biases are calculated for 1980-1999 except for UKMO reanalyses which are shown for 1992-2001. Biases are calculated relative to the ERA-40 reanalyses. For ozone and water vapour, the climatological means and biases are calculated for 1991-2002 except for EMAC and UMETRAC which are shown for 1991-2000. The grey areas show ERA-40 and HALOE plus and minus two standard deviations about the climatological means. The solid black lines indicate the multi-model mean (MMM) results. For other data sets, see legend. Model acronyms are described in Table 1.1 and details for each model are given in Chapter 2.

warm bias (due to larger ozone solar heating) while overestimation of water vapour should generally lead to a cold bias (due to larger infrared cooling), and *vice versa*. Thus, inter-comparison of model results for temperature on the one hand and ozone and water vapour on the other hand provides some guidance as to whether model temperature biases are due to biases in the abundance of these chemical species or due to inaccuracies in the radiation schemes.

A model's ability to reproduce the observed temperature climate does not ensure an accurate sensitivity to perturbations, such as increasing GHGs and ozone depletion. Therefore, we assess model temperatures and model temperature trends separately. The model temperature climatologies are discussed in Section 3.3.1 and the model

temperature trends for the past and future are discussed in Sections 3.3.2 and 3.3.3, respectively.

The analyses presented for the climatology and the past trends are based on model results from the REF-B1 scenario, including observed surface forcings of sea surface temperatures (SSTs), greenhouse gases (GHGs) and ozone depleting substances (ODSs), and variations in volcanic aerosols and solar forcing. To asses future trends, however, model results for the REF-B2 scenario are used. The REF-B2 experiments include, for the past, the same-surface forcing of GHGs and ODSs as REF-B1 but do not include variations in volcanic aerosol and solar forcing. For a complete description of the REF-B1 and REF-B2 scenarios see Chapter 2. For models that have provided multiple ensemble members (for REF-B1: CMAM, CNRM-ACM, LMDZrepro, MRI, SOCOL and WACCM) the results presented show the ensemble mean values, unless stated otherwise.

3.3.1 Global mean temperature climatology

Figure 3.1a shows global mean vertical temperature profiles averaged over 1980-1999 for both the REF-B1 model experiments and for three reanalyses data sets, the latter including ERA-40, NCEP and UKMO (note that the UKMO climatology is derived for 1992-2001). The grey shaded area shows ERA-40 plus and minus two standard deviations about the climatological mean, indicating the interannual variability of this data set. All models capture the large scale features of the troposphere and stratosphere, with decreasing temperatures with height in the troposphere, a distinct temperature minimum at the tropopause around 100 hPa and increasing temperature with height in the stratosphere. The spread between the models is larger in the stratosphere than in the troposphere. Figure 3.1d shows model biases with respect to the ERA-40 climatology. NCEP and UKMO are generally close to ERA-40, but are up to 3 K warmer around the tropopause (near 100 hPa) and up to 6 K warmer in the upper stratosphere. Most models agree well with the observations and are generally within ±5 K of the ERA-40 temperatures. Exceptions are the temperatures from CAM3.5, CCSRNIES, CMAM, CNRM-ACM, LMDZrepro, UMUKCA-METO and UMUKCA-UCAM. CAM3.5, with an upper model boundary at 3 hPa, provides data only up to 5 hPa where it under-estimates temperatures by up to 9 K. CCSRNIES has a cold bias around the tropopause that maximises at -9 K near 70 hPa, and a positive bias of up to 8 K in the middle and upper stratosphere. CMAM displays a similar positive bias of up to 9 K in the middle and upper stratosphere. CNRM-ACM has a cold bias throughout the stratosphere with maximum values of -11 K and -15 K in the lower and upper stratosphere, respectively. LMDZrepro has a warm bias of up to 15 K in the upper stratosphere. UMUKCA-METO and UMUKCA-UCAM both display a distinct warm bias of up to 7-8 K in the lower stratosphere, and UMUKCA-UCAM has a warm bias of up to 6 K in the upper stratosphere. Finally it can be noted that the multi-model mean (MMM) results fall within the ERA-40 interannual variability limits above about 70 hPa, *i.e.*, throughout most of the stratosphere. Below 70 hPa, particularly in the upper troposphere between 300 and 100 hPa, there is a general tendency for the models to have a cold bias. These results are roughly in agreement with the previous multi-model temperature assessment, performed for CCMVal-1 (Austin *et al.*, 2009).

Below follows a qualitative assessment that attempts to identify which features of the temperature biases highlighted above are associated with biases in ozone and water vapour. Models without a clear connection between temperature biases on the one hand, and ozone and water vapour biases on the other, are as discussed earlier likely to have deficiencies in their radiation scheme. Note that the focus here is on explaining features in the temperature fields, not in ozone or water vapour, which are dealt with separately in Chapter 6. Also note that inferences in this section are suggestive. The methodology cannot rule out unknown reasons for model biases. For example, effects of different treatments of clouds and aerosols may have a significant impact on the results in the lower stratosphere, but are not considered in the following analysis.

A more detailed assessment of the radiation scheme performances based on radiative fluxes and heating rates is given in Section 3.4. The combined effect of errors in heating rates and distribution of radiatively active gases on biases in the global mean temperature climatology is analysed in Section 3.4.6.

Figures 3.1b and 3.1c show global mean vertical ozone and water vapour profiles averaged over 1991-2002 for the REF-B1 model experiments and for HALOE observations. Figure 3.1e and 3.1f show model biases with respect to the HALOE climatology. The grey shaded areas show the HALOE plus and minus two standard deviations about the climatological mean.

For ozone, model values are generally within ±1 ppm of the observations, with a tendency for the models to overestimate ozone in the lower stratosphere and to underestimate ozone in the upper stratosphere. The multi-model mean results fall well within the HALOE interannual variability limits throughout the stratosphere and upper troposphere. For water vapour, the inter-model spread is much larger, and biases with respect to the observed climatology are in some cases in excess of 50% of the climatological values themselves. The multi-model mean results underestimate the observations by about 1 ppm in the stratosphere, but are within the HALOE interannual variability limits in this region. Generally, ozone biases are expected to have a larger impact on the temperature than biases in

water vapour, since the longwave radiative effect of water vapour generally is overshadowed by that from CO_2 (an exception is the lower stratosphere, see *e.g.*, Fomichev 2009). However, water vapour biases as large as those presented here can have a significant effect on the radiative balance throughout the stratosphere. For example, in CMAM the inclusion of water vapour cooling in the upper stratosphere leads to a temperature reduction of about 5 K in this region (Fomichev *et al*., 2004), which suggests that large water vapour biases could have a significant impact throughout the stratosphere. Notably, all the models with a significant warm bias in the middle to upper stratosphere (CCSRNIES, CMAM and LMDZrepro) display significant negative biases in water vapour.

CAM3.5 water vapour biases are small (Figure 3.1f), and a large overestimation of ozone mixing ratios in excess of 1 ppm near the model upper boundary (Figure 3.1e), which should lead to overestimated solar heating, seems inconsistent with the CAM3.5 cold bias in this region. Hence the cold bias for this model above 10 hPa is likely to be due to inaccuracies in the model's radiative scheme or possibly associated with the low upper boundary.

CCSRNIES displays the largest bias in water vapour of all models. The model under-estimates the observed values by 2-4 ppm in the middle and upper stratosphere, which likely explains a significant fraction of the model's warm bias in this region. CCSRNIES also overestimates ozone near its peak in the middle stratosphere by almost 2 ppm, which should also contribute to the warm bias. Thus, it is possible that the warm bias in the middle stratosphere is due to biases in ozone and water vapour alone, while in the upper stratosphere, where the model simulation of ozone is quite adequate, the water vapour bias is unlikely to be responsible for the entire 8 K bias there. Also, the cold bias in the lower stratosphere and upper troposphere, cannot be linked to biases in ozone and water vapour, and thus is likely due to inaccuracies in the model's radiative scheme.

CMAM displays a similar positive temperature bias to that of CCSRNIES in the middle and upper stratosphere. While CMAM under-estimates water vapour by about 1 ppm throughout the stratosphere, which should lead to somewhat under-estimated infrared cooling, this can only explain a small fraction of the CMAM warm bias. Furthermore, the fact that CMAM under-estimates ozone slightly in this region, which should lead to reduced solar heating, suggests that the CMAM warm bias in this region is likely to be primarily due to inaccuracies in the model's radiative scheme.

CNRM-ACM ozone biases are small, and although a 1 ppm positive bias in water vapour throughout the stratosphere should contribute to a somewhat overestimated infrared cooling, the bulk of the cold bias in this model is likely to be due to inaccuracies in the model's radiative scheme.

LMDZrepro displays similar biases as CMAM, with overestimated upper stratospheric temperatures, a slight low ozone bias in the upper stratosphere, and a negative bias in water vapour throughout the stratosphere. Although the water vapour bias for LMDZrepro is significantly stronger than for CMAM, amounting to 2-3 ppm, this bias is not sufficient to explain the large warm bias in the upper stratosphere. This and the fact that LMDZrepro agrees well with observed temperatures below 5 hPa (despite a large water vapour bias there) suggests that inaccuracies in the model's radiative scheme should be the main cause for the

Table 3.2: Model temperature climatology bias (K) with respect ERA-40 for 1980-1999 at 70, 15 and 2 hPa. Values in parentheses show the bias in units of ERA-40 one standard deviation interannual variability (70 hPa: 0.65 K; 15 hPa: 0.65 K; 2 hPa: 2.20 K). Sigma values for grading purposes are defined as the maximum differences between the reanalyses data sets and are presented in the last line.

	70 hPa	15 hPa	2 hPa		70 hPa	15 hPa	2 hPa
AMTRAC3	-0.98 (-1.51)	1.81 (2.77)	1.64 (0.74)	SOCOL	-4.39 (-6.73)	-0.29 (-0.44)	-2.54 (-1.15)
CAM3.5	-3.04 (-4.67)	-1.35 (-2.07)	NA	ULAQ	0.71 (1.09)	1.24 (1.89)	2.80 (1.27)
CCSRNIES	-7.45 (-11.4)	4.49 (6.88)	6.00 (2.73)	UMETRAC	-2.97 (-4.56)	-1.91 (-2.93)	2.83 (1.29)
CMAM	1.29 (1.98)	2.28 (3.49)	8.30 (3.78)	UMSLIMCAT	1.37 (2.11)	-0.46 (-0.70)	-0.88 (-0.40)
CNRM-ACM	-9.64 (-14.8)	-6.76 (-10.4)	-10.30 (-4.69)	UMUKCA-UCAM	7.74 (11.87)	0.85 (1.31)	5.39 (2.45)
EMAC	-3.19 (-4.89)	-1.49 (-2.27)	0.40 (0.18)	UMUKCA-METO	7.13 (10.95)	-0.34 (-0.51)	2.62 (1.19)
E39CA	1.99 (3.05)	1.74 (2.67)	NA	WACCM	-0.59 (-0.90)	-0.13 (-0.21)	-0.03 (-0.01)
GEOSCCM	0.53 (0.82)	0.49 (0.75)	2.77 (1.26)	MMM	-0.92 (-1.41)	-0.19 (-0.29)	1.54 (0.70)
LMDZrepro	0.10 (0.15)	-0.65 (-0.99)	11.10 (5.05)	NCEP	0.74 (1.13)	0.95 (1.46)	3.23 (1.47)
MRI	-0.99 (-1.53)	-2.88 (-4.41)	-2.60 (-1.18)	UKMO	-0.18 (-0.27)	-0.99 (-1.51)	1.30 (0.59)
NiwaSOCOL	-4.14 (-6.36)	-0.01 (-0.01)	-2.85 (-1.29)	Sigma	0.74 (1.13)	-0.99 (-1.51)	3.23 (1.47)

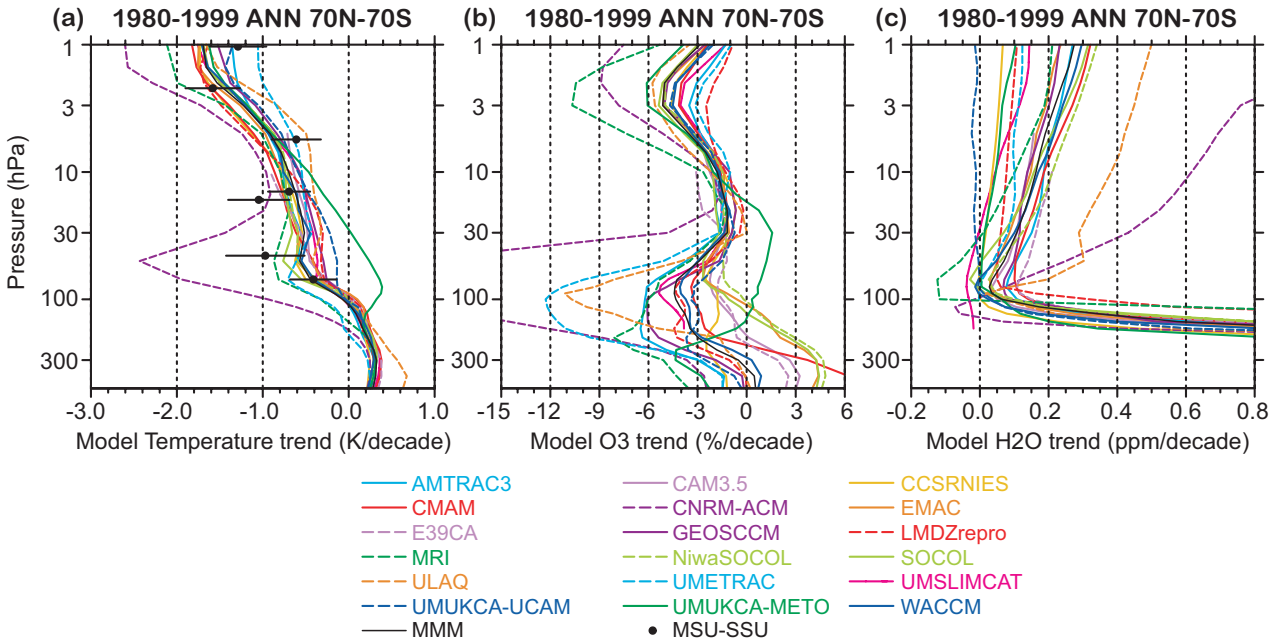

Figure 3.2: Near global (70°S-70°N) and annual mean trends over 1980-1999 for (a) temperature, (b) ozone, and (c) water vapour ratio, for REF-B1 model simulations. Panel (a) includes satellite observed MSU/SSU trends and 95% confidence intervals. MSU/SSU data points include channels: MSU-4 (at 70 hPa), SSU25 (15 hPa), SSU26 (5 hPa), SSU27 (2 hPa), SSU15X (45 hPa), SSU26X (15 hPa) and SSU36X (1 hPa), where the specified pressure levels represent the approximate weighted mean heights derived from the MSU/SSU vertical weighting functions for each channel (see Randel et al., 2009), negative portions of the weighting functions excluded. The solid black lines indicate the multi-model mean (MMM) results. For other data sets, see legend.

LMDZrepro temperature bias.

UMUKCA-METO and UMUKCA-UCAM overestimate ozone in the lower stratosphere, which should lead to overestimated radiative heating. This provides a plausible explanation for the UMUKCA-METO and UMUKCA-UCAM warm biases in this region, although other effects cannot be ruled out.

Table 3.2 shows model temperature climatology biases with respect ERA-40 for 1980-1999 at 70, 15 and 2 hPa. Sigma values for grading purposes are defined as the maximum differences between the reanalyses data sets and are also presented in Table 3.2 (see Section 3.6).

3.3.2 Global mean temperature trends: Past

Figure 3.2 shows near global mean trends for temperature, ozone and water vapour from 1980-1999 for the REF-B1 model experiments. Trends were calculated from linear fits to the annual mean time series from each model. Figure 3.2a also shows the observed stratospheric temperature trend over this period, indicated by the MSU/SSU dataset. The horizontal error bars for MSU/SSU indicate the 95% confidence intervals for the fitted trends. Note that MSU/SSU data are also associated with uncertainty in the vertical due to the vertical distribution of its weighting functions (see Randel *et al*., 2009). Here the MSU/SSU data was simply plotted at the weighted mean heights (negative portions of the weighting functions excluded). Since the focus in this analysis is on temperature no observations are included in Figure 3.2 for ozone and water vapour, and thus the following qualitative assessment will use the multi-model mean as a reference for these species.

The observed temperature trend is associated with emission of CO_2 and ozone depleting substances (Jonsson *et al*., 2009) and is driven radiatively by increases in CO_2 and water vapour and decreases in ozone (Shine *et al*., 2003). All models capture the large scale features of the observed temperature trend, with warming in the troposphere (not shown) and cooling in the stratosphere. Furthermore, the vertical structure of the stratospheric trend, with cooling maxima in the upper and lower stratosphere that are consistent with decreases in ozone (Figure 3.2b), is generally well captured. The following discussion will primarily focus on the stratospheric results. Disregarding the main model outliers in the stratosphere, CNRM-ACM and UMUKCA-METO, the model spread varies between 0.4 K/decade and 0.8 K/decade. In the deep troposphere (below 300 hPa) the models agree better, and except for the main outlier there, ULAQ, the model spread is within 0.2 K/decade. The multi-model mean results overlap with, or

are very close to overlapping with, the MSU/SSU uncertainty estimates, and the disagreements are largest for the so called SSU X-channels that are not as reliable as the regular SSU channels. Note that many models with significant biases in the temperature climatology (see Section 3.3.1), including CCSRNIES, CMAM, LMDZrepro and CAM3.5, do not show a significant disagreement with the observed trends. Some models, however, and most notably CNRM-ACM and UMUKCA-METO, but also MRI, UMETRAC, UMUKCA-UCAM and ULAQ, display trends that are in sufficient disagreement with the observations and the multi-model mean trend that they warrant some further investigation.

CNRM-ACM overestimates the observed cooling trend throughout most of the stratosphere and exhibits cooling, rather than warming, in the upper troposphere (Figure 3.2a). The discrepancies are particularly severe near the stratopause and in the lower stratosphere and upper troposphere, between 200 and 20 hPa, where the modelled trend is a roughly factor of 1.5 and 4, respectively, greater than the multi-model mean trend. The overestimated temperature trend is quite clearly associated with a significantly overestimated negative ozone trend (Figure 3.2b) and a significantly overestimated positive water vapour trend (Figure 3.2c), both leading to overestimated cooling. A particularly strong temperature response to volcanic eruptions in 1982 an 1991 (Figure 3.3) appears to be partly responsible for these anomalous trends.

MRI also overestimates the temperature trend near the stratopause and in the lower stratosphere and upper troposphere, although to a lesser degree than CNRM-ACM. This appears to be associated with too strong negative ozone trends.

UMETRAC displays a stronger temperature trend than most models in the upper troposphere and lower stratosphere and a weaker trend than most models in the upper stratosphere. This seems consistent with slightly stronger and weaker ozone trends than most models in these regions.

UMUKCA-METO displays an anomalous feature with a weaker than average temperature trend in the middle stratosphere and a positive trend of up to 0.4 K/decade in the lower stratosphere. This behaviour seems directly related to an anomalous ozone trend with positive, rather than negative, values throughout the lower and middle stratosphere.

While UMUKCA-UCAM and UMUKCA-METO showed very similar results for the temperature and ozone climatologies and biases (Figure 3.1), this is not the case for temperature trends. UMUKCA-UCAM performs well throughout the domain, except for a slightly weaker than average trend in the lower stratosphere, which appears consistent with the absence of a significant negative water vapour trend and a slightly weaker than average negative ozone trend in this region.

ULAQ displays somewhat weaker negative temperature trends than the other models at 20-2 hPa, despite showing reasonable ozone trends in this region and an overestimated water vapour trend. As the latter would lead to more cooling, not less, this suggests that the lower than average sensitivity for this model at 20-2 hPa could be due to inaccuracies in the model's radiative scheme. Also, although the focus here is on the stratosphere, it can be noted that the upper tropospheric warming in ULAQ is much stronger than for other models (by roughly a factor of 2 below 300 hPa). This appears to be related to an upper tropospheric increase in water vapour that is about twice as strong as for the multi-model mean (not shown).

Figure 3.3 shows the full time series of global mean temperature anomalies compared to satellite data weighted over specific vertical levels (see Randel *et al*., 2009). Most of the models capture the observed trends and variability. In particular many CCMs capture the levelling of the temperature since the late 1990s. The impact of the prescribed SSTs in the troposphere is also apparent as MSU-4 and model temperatures are particularly well correlated compared to other levels.

A disagreement between the models and observations is clearly seen in SSU26 over the last decade. SSU26 has a maximum weight at about 5 hPa and a considerable contribution from the lower stratosphere. In contrast the agreement is better in SSU27 which peaks at 2 hPa with less contribution from the lower stratosphere.

Table 3.3 shows the CCM temperature trend bias (K/decade) with respect MSU/SSU for 1980-1999 at 70, 15 and 2 hPa. 95% confidence intervals in the MSU/SSU trend are used for grading purposes (see Section 3.6). These are also presented in the table.

3.3.3 Global mean temperature trends: Future

To assess the model simulations of future changes **Figures 3.4c** and d show global mean vertical temperature trend profiles for 2000-2049 and 2050-2099 for the REF-B2 model experiments. For reference, the global mean trends for 1980-1999 for REF-B1 and REF-B2 are shown in Figures 3.4a and b. We first compare the REF-B2 and REF-B1 results for 1980-1999. The REF-B2 results are generally very similar to the REF-B1 results in the stratosphere, as should be expected since the prescribed changes of GHGs and ODSs are the same in both scenarios. The multi-model mean trends for REF-B1 and REF-B2 are very close. However, there are a few important differences that are discussed below.

While the focus here is on the stratospheric results it can be noted that three models show significantly different temperature trends in the upper troposphere for REF-B2

than for REF-B1. CMAM and UMUKCA-UCAM REF-B2 trends are roughly 1.5 and 2 times as strong as the multi-model mean trend in this region. For CMAM this is related to its coupled ocean implementation, which is documented elsewhere in the report. CCSRNIES shows the opposite behaviour, *i.e.*, under-estimating the multi-model trend, showing a near zero trend throughout the troposphere for REF-B2.

For the stratosphere, the REF-B2 trends show slightly better agreement between the various models than for REF-B1 (but note that not all models provided data for REF-B2). This is not surprising as the variation in model response to volcanic eruptions and solar variability contributes to different temperature responses in the REF-B1

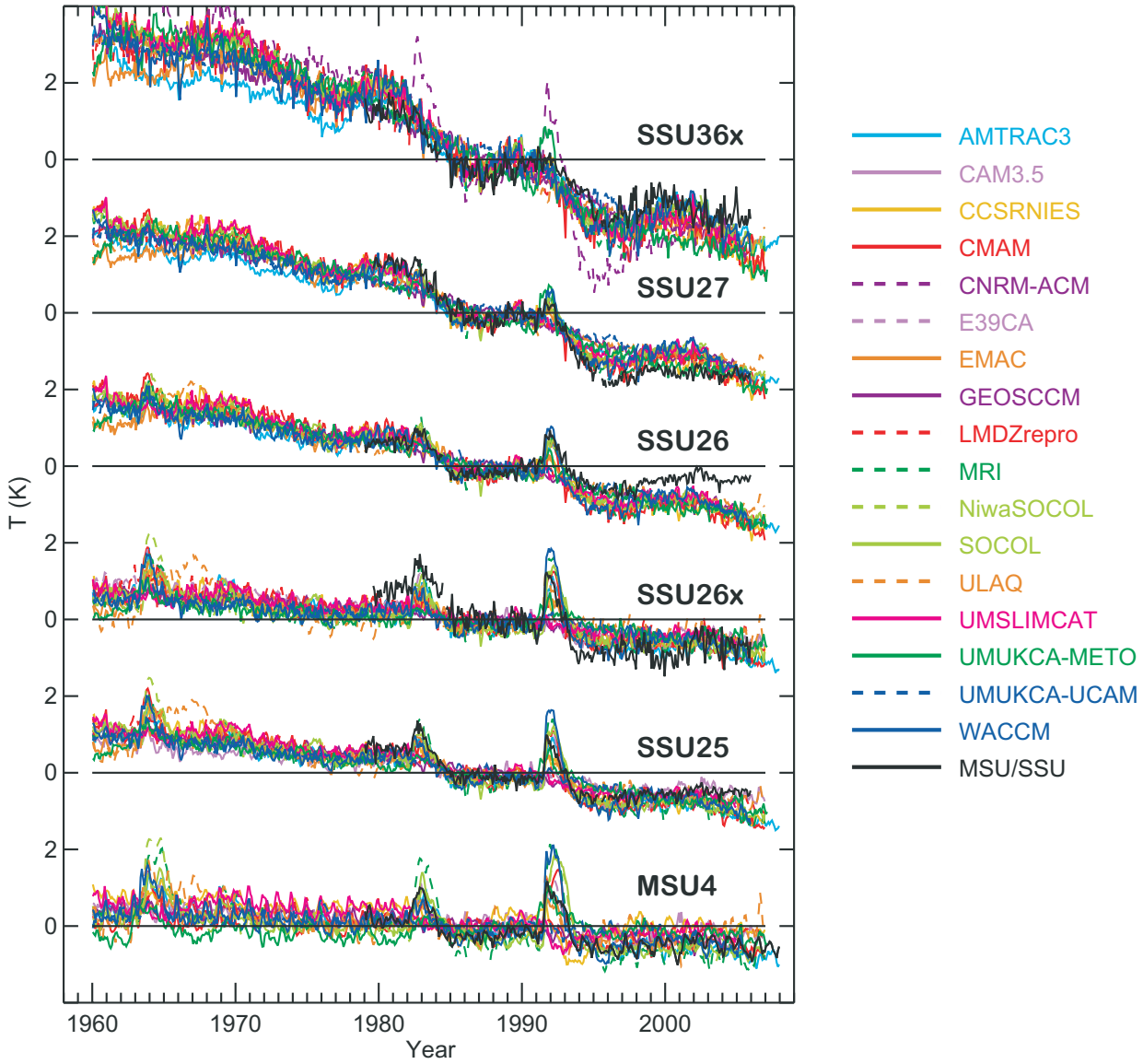

Figure 3.3: Near global mean time series (70°S-70°N) of MSU/SSU satellite observations and REF-B1 model temperature data weighted by MSU/SSU weighting functions. MSU/SSU channels include: MSU-4 (at 70 hPa), SSU25 (15 hPa), SSU26 (5 hPa), SSU27 (2 hPa), SSU26x (15 hPa) and SSU36x (1 hPa), where the specified pressure levels represent the approximate weighted mean heights derived from the MSU/SSU vertical weighting functions for each channel (see Randel et al., 2009), negative portions of the weighting functions excluded. For each model only the first ensemble member from the REF-B1 simulations is shown. The anomalies are calculated with respect to the period 1980-1994, as in the provided SSU anomalies. Note that UMETRAC is not included in this figure. CNRM-ACM is only shown in the highest SSU36x level due to its too strong sensitivity to volcanoes. UMUKCA-UCAM in not shown after year 2000. Low top models CAM3.5 and E39CA (the lids are at 3 hPa and 10 hPa respectively) are shown only in the MSU4, SSU25 and SSU26x panels.

Table 3.3: Model temperature trend bias (K/decade) with respect MSU/SSU for 1980-1999 at 70, 15 and 2 hPa. Values in parentheses show biases in units of the MSU/SSU 95% confidence intervals (70 hPa: 0.27 K/decade; 15 hPa: 0.24 K/decade; 2 hPa: 0.32 K/decade). The Sigma values used for grading purposes are presented in the last line.

	70 hPa	15 hPa	2 hPa		70 hPa	15 hPa	2 hPa
AMTRAC3	0.02 (0.08)	-0.03 (-0.14)	0.31 (0.99)	NiwaSOCOL	0.03 (0.10)	0.01 (0.03)	0.16 (0.49)
CAM3.5	0.14 (0.53)	0.11 (0.47)	NA	SOCOL	-0.14 (-0.52)	-0.03 (-0.14)	0.16 (0.51)
CCSRNIES	-0.09 (-0.33)	0.03 (0.12)	-0.01 (-0.02)	ULAQ	0.08 (0.31)	0.29 (1.18)	0.43 (1.34)
CMAM	0.10 (0.37)	-0.08 (-0.34)	-0.01 (-0.04)	UMETRAC	-0.30 (-1.10)	0.17 (0.68)	0.62 (1.94)
CNRM-ACM	-1.53 (-5.66)	-0.22 (-0.91)	-0.57 (-1.79)	UMSLIMCAT	0.03 (0.13)	0.19 (0.78)	0.18 (0.56)
EMAC	0.01 (0.04)	-0.07 (-0.28)	0.07 (0.21)	UMUKCA-METO	0.77 (2.85)	0.38 (1.54)	0.20 (0.62)
E39CA	0.09 (0.35)	-0.12 (-0.48)	NA	UMUKCA-UCAM	0.27 (1.01)	0.22 (0.88)	0.31 (0.97)
GEOSCCM	0.15 (0.57)	0.18 (0.75)	0.27 (0.86)	WACCM	0.00 (0.01)	0.07 (0.30)	0.19 (0.58)
LMDZrepro	0.12 (0.46)	0.19 (0.78)	-0.06 (-0.18)	MMM	-0.03 (-0.13)	0.07 (0.28)	0.12 (0.38)
MRI	-0.40 (-1.49)	-0.05 (-0.20)	-0.28 (-0.88)	Sigma	0.27 (1.0)	0.24 (1.0)	0.32 (1.0)

simulations, while those effects are not considered for REF-B2.

CNRM-ACM shows the most dramatic difference in temperature trends between REF-B1 and REF-B2 of all models. The considerably overestimated cooling trends for 1980-1999 for REF-B1 are much reduced in REF-B2, particularly in the lower stratosphere. This confirms the earlier speculations that the CNRM-ACM temperature trend biases for REF-B1 are largely due to effects of volcanic eruptions, since the REF-B2 simulation does not include those. It can be speculated that the particularly large model spread for REF-B1 in the lower stratosphere, including significant deviations also for MRI, UMETRAC, UMUKCA-METO and UMUKCA-UCAM, could be related to different responses to volcanic eruptions. Note that for REF-B2, except for UMUKCA-METO and UMUKCA-UCAM, the model spread is quite small. Further work is needed to understand this better. MRI shows better agreement with the multi-model mean for REF-B2 than for REF-B1, particularly in the upper troposphere and lower stratosphere. UMUKCA-UCAM on the other hand showed better agreement with the multi-model mean (and with the observations) for REF-B1 than for REF-B2. For REF-B2, UMUKCA-UCAM follows the anomalous results of UMUKCA-METO, showing a strong positive bias in its temperature trend throughout the lower and middle stratosphere.

The future global mean temperature trend is attributable primarily to CO_2 increase, although the expected gradual recovery of ozone over the 21st century will reduce the CO_2 induced cooling somewhat in the upper stratosphere (Jonsson *et al*., 2009). A hint of this can be seen in Figures 3.4c and d. For 2000-2049 (Figure 3.4c) only two models can be considered as significant outliers: MRI under-estimates the multi-model cooling trend in the upper stratosphere and ULAQ overestimates the multi-model warming trend in the upper troposphere. In particular the anomalous behaviour of UMUKCA-METO and UMUKCA-UCAM in the lower stratosphere is not present in this period. CMAM and UMUKCA-UCAM tropospheric trends are also closer to the multi-model mean trend. MRI did not include CH_4 changes after 2002 (see Chapter 2) which would explain weaker temperature trend for MRI in the upper stratosphere than for other models (CH_4 is the main source of upper stratospheric water vapour and odd hydrogen that control ozone loss rates in this region). For 2050-2099 (Figure 3.4d) the same level of agreement between the models is achieved in the stratosphere. In the troposphere, however, the model spread is larger during 2050-2099 than during 2000-2049. In particular, SOCOL shows a more anomalously warm trend during 2050-2099 than during 2000-2049.

3.4 Evaluation of the CCM radiation codes performance

There is a long history of international efforts aimed on the evaluation of the radiation codes of climate models. After several national projects in Europe, Russia and US (*e.g*., Feigelson and Dmitrieva, 1983; Luther *et al*., 1988) the first international comparison of radiation codes for climate models (ICRCCM) campaign was launched in 1984. ICRCCM resulted in a series of publications (Ellingson *et al*., 1991; Fouquart *et al*., 1991) that evaluated the performance of the existing radiation codes and inspired further progress. ICRCCM also established a framework for the subsequent campaigns, based on the comparison of the radiation codes against reference high-resolution line-by-line (LBL) codes. This approach was justified by the unavailability of reliable observations of the radiation fluxes

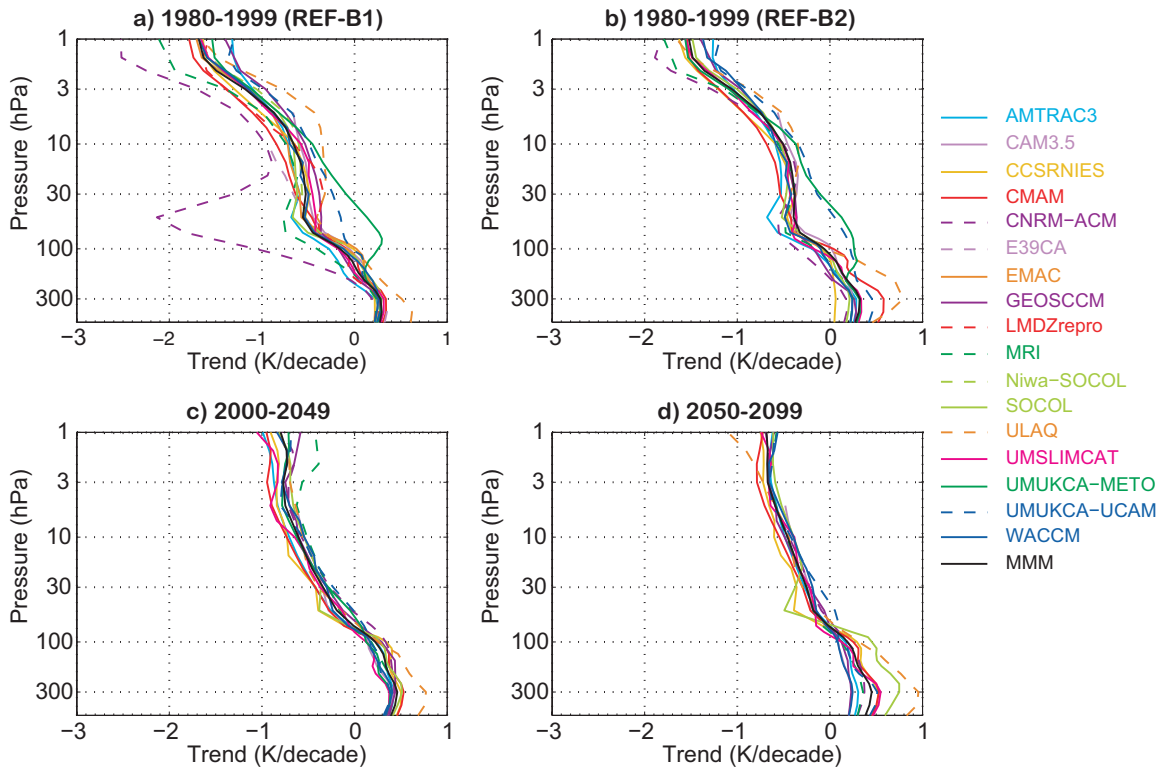

Figure 3.4: Global and annual mean temperature trends from (a) REF-B1 for 1980-1999; and from REF-B2 for (b) 1980-1999, (c) 2000-2049, and (d) 2050-2099. Note that UMETRAC is not included in this plot and that four models shown for REF-B1 (EMAC, E39CA, LMDZrepro and NiwaSOCOL) did not supply data for REF-B2. The solid black lines indicate the multi-model mean (MMM) results.

and heating rates in the atmosphere. There were several other attempts to evaluate radiation codes for climate models. The representation of clouds was analysed by Barker *et al*., (2003). An evaluation of clear sky radiation codes used by IPCC AR4 GCMs was performed by Collins *et al*., (2006), employing a single profile and solar zenith angle. These evaluations were also based on the comparison of operational radiation codes with reference LBL schemes. Such tests can provide a useful, if incomplete, understanding of potential sources of uncertainty and error, because the state-of-the art LBL radiation codes are used as a base for the judgment. A more complete picture can be obtained by comparing radiation codes directly implemented to a single climate model (*e.g*., Feigelson and Dmitrieva, 1983; Cagnazzo *et al*., 2007). However, it would not be feasible to apply this approach using the LBL reference codes due to their high computational costs and, moreover, the results of offline experiments allow clear evaluation of the model performance and interpretation of the underlying causes of error.

Most of the previous campaigns were aimed at the radiation fluxes and tropospheric heating/cooling rates evaluation. In this comparison we focus on two aspects of radiation code output: stratospheric heating/cooling rates and instantaneous radiative fluxes. The heating/cooling rates are necessary to understand the biases and trends in the global mean stratospheric temperature, while the instantaneous radiative fluxes can help to interpret global climate change, including surface temperature change. It should be noted that the evaluation of radiation codes in cloudy conditions and in the presence of different atmospheric aerosols will not be performed here, because of high uncertainties in aerosol optical properties and limited availability of proper reference codes. Nevertheless, these issues are very important and should be addressed in future work.

In this section we analyse the performance of the CCM radiation codes presented in Section 3.2 and described in Chapter 2 using the results of offline calculations. Section 3.4.1 describes the cases required for this analysis. Sections 3.4.2 and 3.4.4 evaluate the performance of CCM radiation codes for the control case (case A, see Section 3.4.1), for fluxes and heating/cooling rates, respectively, which can help to explain the possible causes of the biases in the CCM simulated climatological temperature discussed in Section 3.3. Sections 3.4.3 and 3.4.5 evaluate the response of the simulated radiation fluxes and heating rates, respectively, to the changes of atmospheric gas composition and Section 3.4.6 discusses the effect of errors in heating rates and distribution of ozone and water vapour on biases in the global mean temperature climatology.

3.4.1 Experimental set-up

We perform a number of clear sky and aerosol free tests using zonally averaged profiles of the atmospheric state parameters compiled from ECMWF ERA-40 output and ozone data provided by Randel and Wu (2007). These profiles represent January atmosphere and are given for five latitudes (80°S, 50°S, 0°, 50°N, and 80°N). The solar fluxes in the atmosphere were calculated for three solar zenith angles, allowing one to evaluate the radiation code performance for diurnal means as well as for different solar positions. Where possible the extra-terrestrial spectral solar irradiance was prescribed with ~1 nm resolution from Lean *et al*. (2005) compilation. Surface albedo was set to 0.1 for all cases. We also asked participants to use solar irradiance for 1 AU Sun-Earth distance. The set of reference vertical profiles and the description of the test cases are presented at ***www.env.leeds.ac.uk/~piers/ccmvalrad.shtml***. These tests were designed to very crudely approximate the radiative forcing evolution since 1980 due to ozone and greenhouse gases. **Table 3.4** describes the experiments undertaken. Case A represents the control experiment and is based on the concentration of radiatively active species for 1980. The cases B-L are based on the observed changes of gas abundances in the atmosphere from 1980 to 2000 and allow us to evaluate the radiation code response to these climate forcings.

As a base for comparison we use the results of five LBL codes: AER (Clough and Iacono, 1995; Clough *et al*., 2005); FLBLM (Fomin and Mazin, 1998; Fomin, 2006; Halthore *et al*., 2005); LibRadtran (Mayer and Kylling, 2005); NOAA (Portmann *et al*., 1997) and OSLO (Myhre and Stordal, 1997, 2001; Myhre *et al*., 2006). AER, FLBLM, NOAA and OSLO provided longwave (LW) fluxes, while shortwave (SW) fluxes were calculated with FLBLM, LibRadtran and OSLO codes. Therefore, for most of the cases the results of at least three independent LBL codes are available. The complete set of the test calculations was submitted by the following thirteen CCMs: AMTRAC3, CCSRNIES, CMAM, E39CA, EMAC, GEOSCCM, LMDZrepro, MRI, SOCOL, NiwaSOCOL (identical to SOCOL), UMSLIMCAT, UMUKCA-METO, and UMUKCA-UCAM. Five CCMs (CAM3.5, CNRM-ACM, ULAQ, UMETRAC, and WACCM) did not participate in the radiation code comparison. Two CCMs have radiation codes based on ECHAM4 (E39CA and SOCOL). In addition to the operational codes, we also analysed the results of four perspective radiation codes: ECHAM5, LMDZ-new, UKMO-HADGEM3 and UKMO-Leeds, which will be used in the new generation of CCMs or GCMs.

3.4.2 Fluxes: Control experiment

The global and diurnal mean net (downward minus upward) LW, SW and total (SW+LW) fluxes for case A calculated with AER (LW) and LibRadtran (SW) at 200 hPa (the pseudo-tropopause) are presented in **Table 3.5**. The differences between the fluxes calculated with all participating models and two particular LBL codes (AER for LW and LibRadtran for SW) at the pseudo-tropopause are illustrated in **Figure 3.5**. For this particular case the accuracy of the calculated SW fluxes is very good. The scatter among the LBL codes is within 1 W/m^2. Most of the participating CCMs show a net SW flux error smaller than 2.5 W/m^2. Only the SW radiation scheme of MRI produces a larger error, ~4 W/m^2. For LW and total radiation the situation is slightly worse. While LBL codes are in a very good agreement, total flux errors for GEOSCCM, LMDZrepro and CCSRNIES exceed 4 W/m^2, primarily due to errors in LW calculations. MRI and UMSLIMCAT also display a total flux error of ~4 W/m^2, which is due to either SW errors (for MRI) or a combination of SW and LW errors (for UMSLIMCAT). In general, an error of ~4 W/m^2 could lead to ~4 K error in the global mean surface temperature, unless this error is compensated by some other bias in the concentrations of radiatively active gases or physical parameterisations in the core CCM. It is interesting to note, that for UMUKCA-METO, UMUKCA-UCAM and UKMO-Leeds the SW and LW errors compensate each other making the model performance for the total net flux better than for its individual components. From the results

Table 3.4: Offline radiation experiments undertaken.

A) 1980 Control experiment
B) CO_2 from 338 ppm to 380 ppm
C) CH_4 from 1600 ppb to 1750 ppb
D) N_2O from 300 ppb to 320 ppb
E) CFC-11 from 150 ppt to 250 ppt
F) CFC-12 from 300 ppt to 550 ppt
G) All long-lived greenhouse gas changes combined (B-F)
H) 10% stratospheric ozone depletion, for pressures less than 150 hPa
I) 10% tropospheric ozone increase, for pressures greater 150 hPa
J) 10% stratospheric water vapour increase, for pressures less than 150 hPa
K) 10% tropospheric water vapour increase, for pressures greater than 150 hPa
L) Combined stratospheric ozone depletion and greenhouse gas changes (G and H)

presented, it can be concluded that the performance of the majority of participating models in the simulation of the net fluxes at the pseudo-tropopause is very good.

The global and diurnal mean net (downward minus upward) LW, SW and total (SW+LW) fluxes for case A calculated with AER (LW) and LibRadtran (SW) at the surface are presented in the first line of Table 3.5. Deviations from the LBL code are shown in **Figure 3.6**. In general, the model accuracy at the surface is similar to the results at the pseudo-tropopause for LW fluxes. All models except the ECHAM4 family of models (E39CA and SOCOL), CMAM, LMDZrepro and CCSRNIES have relatively small (< 2 W/m^2) biases.

Figure 3.7 illustrates the errors in downward LW fluxes simulated with three of these models relative to the reference AER LBL scheme. The SOCOL radiation scheme overestimates the downward LW flux at the surface by more than 7.5 W/m^2, which leads to an overestimation of the net LW flux, because the upward LW flux is constrained by the prescribed surface temperature and emission efficiency. The overestimation of the downward flux in SOCOL starts from ~250 hPa and its magnitude increases towards the surface, which suggests some problems with the emission by water vapour or its continuum in the atmospheric transparency window. Similar behaviour (perfect agreement in the stratosphere and rising overestimation in the troposphere) is also characteristic for the CCSRNIES model up to ~300 hPa, however, in the lower troposphere CCSRNIES dramatically under-estimates LW downward fluxes, which leads to substantial errors at the surface and potential implications for the surface energy budget in the core CCM. This model deficiency can be connected to some problems in the representation of the strong emission from H_2O rotational ($\lambda > 15$ μm) or vibrational (~6.3 μm) bands. The accuracy of the LMDZrepro LW downward flux is reasonable in the stratosphere and upper troposphere, but in the lower troposphere, and at the surface the model error exceeds 5 W/m^2. It should be noted also that this model generates a jump in the downward LW fluxes around 10 hPa.

The accuracy of the calculated SW net fluxes at the

Table 3.5: Global and diurnal mean net LW, SW and total (LW+SW) fluxes for case A and their deviation for cases B-L from reference case A at the pseudo-tropopause calculated with AER(LW) and LibRadtran (SW). The first line also shows surface fluxes for reference.

Case	LW flux (W/m^2)	SW flux (W/m^2)	Total flux (W/m^2)
A (reference surface)	-71.88	223.77	151.89
A (reference trop)	-234.076	282.444	48.368
B (CO2)	0.815	-0.052	0.763
C (CH4)	0.072	-0.006	0.066
D (N2O)	0.073	-0.0026	0.0704
E (CFC-11)	0.0251	0.0	0.0251
F (CFC-12)	0.078	0.0	0.078
G (LLGHG)	1.063	-0.061	1.002
H (O3 strat)	-0.094	0.34	0.246
I (O3 trop)	0.164	0.006	0.170
J (H2O strat)	0.072	-0.013	0.059
K (H2O trop)	2.258	0.089	2.347
L (LLGHG&O3)	0.971	0.278	1.248

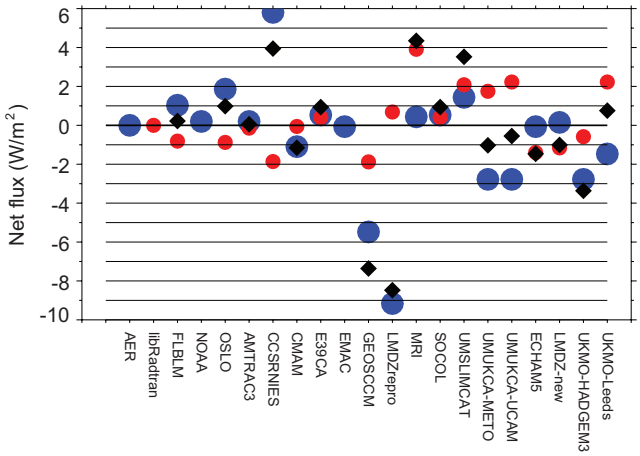

Figure 3.5: The global and diurnal mean SW (red circles), LW (blue circles) and total (black diamonds) net flux deviations from the LBL code (AER for LW and libRadtran for SW) at the model pseudo-tropopause (200 hPa).

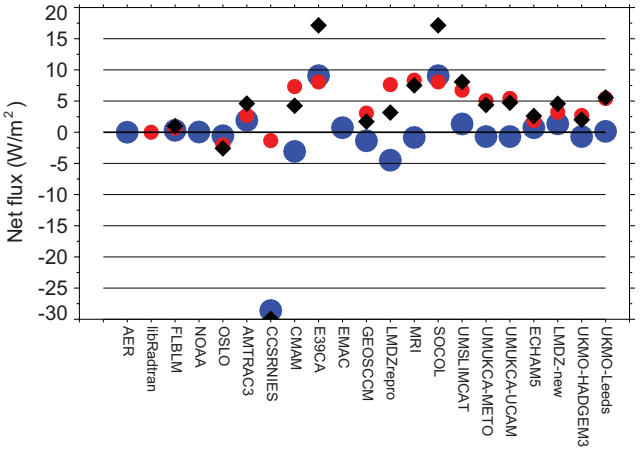

Figure 3.6: The global and diurnal mean SW (red circles), LW (blue circles) and total (black diamonds) net flux deviations from the LBL code (AER for LW and libRadtran for SW) at the surface.

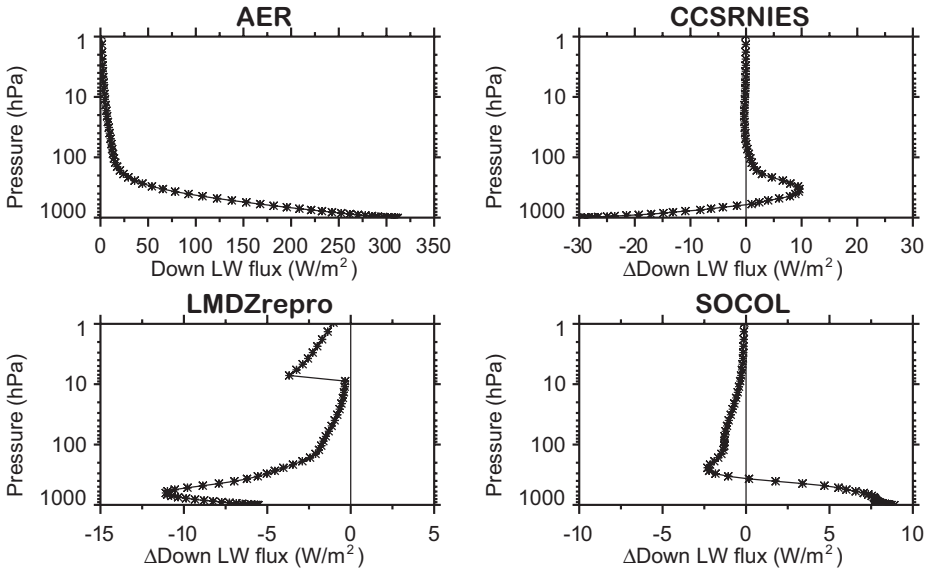

Figure 3.7: The vertical profiles of the global and diurnal mean LW downward flux from the LBL code (AER) and the absolute deviations of SOCOL, LMDZrepro and CCSRNIES results from the reference AER LBL scheme.

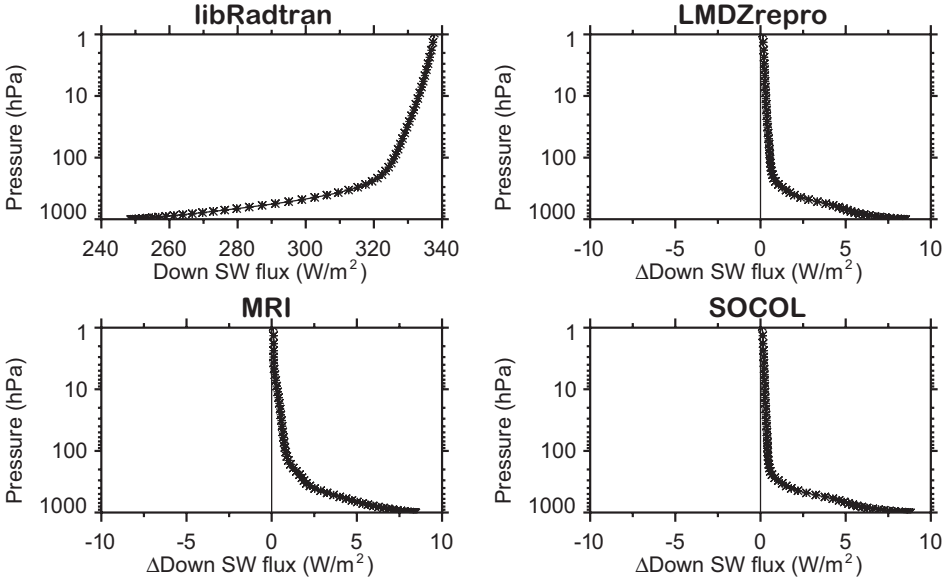

Figure 3.8: The vertical profiles of the global and diurnal mean SW downward flux from the LBL code (lib Radtran) and the absolute deviations of SOCOL, MRI and LMDZrepro results from the reference libRadtran LBL scheme.

surface (Figure 3.6) is generally not as good as at the pseudo-tropopause. For this case only six models (AMTRAC3, CCRSNIES, GEOSCCM, ECHAM5, LMDZ-new and UKMO-HADGEM3) perform well. All other models are biased high compared to the reference LibRadtran results. The magnitude of the bias varies from about 5 to 8 W/m^2 with larger biases for the ECHAM4 family, CMAM, LMDZrepro and MRI. The bias in the SW net fluxes mostly comes from the errors in the downward SW fluxes, because the upward SW fluxes are smaller and constrained by the prescribed surface albedo. The downward SW flux errors in most of the above-listed models have similar behaviour. As illustrated in **Figure 3.8**, the errors are small in the stratosphere, but start to increase around ~200 hPa reaching the maximum value near the surface. Because the main absorber of the solar irradiance in the cloud and aerosol free troposphere is water vapour, it can be tentatively concluded that H_2O absorption in the near-infrared spectral region is under-estimated by these models, although under-estimating O_3 absorption in the visible spectral region also can contribute. The errors in the total net radiation fluxes (Figure 3.6) coincide with the errors in SW net fluxes for most of the models. The exceptions are ECHAM4 family of models, LMDZrepro and CCSRNIES. In ECHAM4

based models the errors in SW and LW net fluxes are almost equal in magnitude providing a substantial deviation of the surface radiation balance from the reference results. The total net flux error for CCSRNIES is very large (~30 W/m^2) and is dominated by the problems in the LW part of the code. The error in total net surface flux for LMDZrepro is rather small due to compensation of the errors in SW and LW calculations.

3.4.3 Fluxes: Sensitivity experiments

The analysis of the radiation flux responses to the observed changes of gas abundances in the atmosphere from 1980 to 2000 is an important part of the radiation code evaluation, because the accuracy of past climate change simulations depends on the ability of the radiation codes to properly simulate the effects of the main climate drivers (Collins *et al*., 2006). In Table 3.5 we present the global and diurnal mean net LW, SW and total flux changes for cases B-L relative to reference case A (for case definitions see Table 3.4) at the pseudo-tropopause simulated with reference LBL codes (AER for LW fluxes and LibRadtran for SW fluxes). The calculated effects of different atmospheric perturbations are generally close to the previous estimates (Collins *et al*., 2006; Forster *et al.*, 2007).

The global and diurnal mean net SW, LW and total flux deviations of the radiative forcing due to CO_2 increase relative to the results of the LBL codes at the pseudo-tropopause are presented in **Figure 3.9**. The accuracy of the LW radiation codes is generally very good and is within 10% for most of the participating models. Slightly larger underestimation of the CO_2 forcing is visible for the ECHAM4 family, CMAM and LMDZrepro, but it does not exceed 20%.

The relatively weak SW solar CO_2 forcing is more difficult to simulate. Only the AMTRAC3 and MRI results are in good agreement with the reference code, while most of the models (except CCSRNIES) overestimate its magnitude. The accuracy is still reasonable (<20%) for the UKMO family of models (UMSLIMCAT, UMUKCA-METO, UMUKCA-UCAM, UKMO-HADGEM3 and UKMO-Leeds), but several other models overestimate the solar CO_2 forcing by up to 80%. CCSRNIES does not include CO_2 in the solar part of the code and therefore underestimates SW forcing by 100%. The total (SW+LW) forcing is dominated by LW forcing. Therefore, the accuracy of the total forcing calculation almost completely coincides with the accuracy of LW forcing. Similar conclusions can be drawn for the accuracy of radiative forcing due to increase of all long-lived greenhouse gases (LLGHG) (**Figure 3.10**) since the forcing magnitude is mostly defined by the CO_2 increase. However, for this case the accuracy of the LW forcing calculations is slightly lower for MRI and LMDZ-new and much higher for CMAM. It can be explained by the error compensation in the latter model, which underestimates LW CO_2 forcing but overestimates the LW forcing by N_2O and CFCs (see **Table 3.6**). It should be noted, that the CCSRNIES code does not take into account all LLGHG in the solar part of the spectrum (Table 2.11).

Figure 3.11 shows the accuracy of the considered radiation codes for case H (10% decrease of stratospheric ozone). In contrast to the previously considered cases, the SW forcing for this case plays a major role and all models are able to simulate its magnitude with an accuracy of 20% or better. The performance of some models in the LW part, however, is poor. The accuracy of AMTRAC3, CCSRNIES, CMAM, EMAC, GEOSCCM, LMDZrepro, MRI, ECHAM5 and LMDZ-new is only around 30% or worse, which has important implications for the total forcing of stratospheric ozone although the SW component dominates the total effect.

The accuracy of the LW radiative forcing due to tropospheric ozone and water vapour increase (cases I and K, not shown) is within 10% for all models except CCSRNIES, which has a problem with the H_2O treatment in the LW part of the spectrum and under-estimates the LW forcing for case K by ~20%. The solar forcing for these cases does not play a substantial role. The results for the case J (stratospheric water vapour increase) are shown in **Figure 3.12**. For this case it is interesting to note ~100% overestimation of the LW stratospheric water vapour forcing by all models from the UKMO family and by ~200% by CCSRNIES. The large spread in stratospheric water vapour forcings was also noticed by Myhre *et al*. (2009). It is even more interesting that the SW forcing by stratospheric water vapour is also roughly two times higher in the UKMO family (except for UMSLIMCAT) than for the reference model.

The accuracy of the forcing calculations for case L (all LLGHG and stratospheric ozone depletion) is illustrated in **Figure 3.13**. This forcing represents the sum of the main climate drivers (except water vapour and tropospheric ozone) for the considered period and its reasonable accuracy is a prerequisite for successful simulation of tropospheric climate changes. The results reveal that most of the models have accuracy of forcing calculations within 10%. The outliers are ECHAM4 based models, LMDZ-new and MRI, which under-estimate the total forcing by more than ~10%.

Table 3.6 presents a summary of total flux and forcing differences compared to the total forcing of the reference case (LibRadtran + AER). The table shows all the individual forcings analysed. Also shown are sigma values for the total cases that are used for grading. One sigma corresponds to the maximum absolute SW difference between the LBL models and LibRadtran added to the absolute maximum LW difference between AER and the other LBL models. See Section 3.6 for grading details.

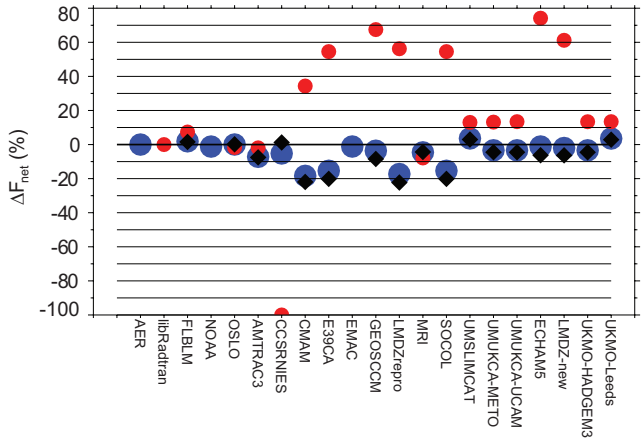

Figure 3.9: The global and diurnal mean SW (red circles), LW (blue circles) and total (black diamonds) net flux deviations of the radiative forcing due to CO_2 (case B) increase relative to the results of LBL codes (AER for LW and libRadtran for SW) at the pseudo-tropopause.

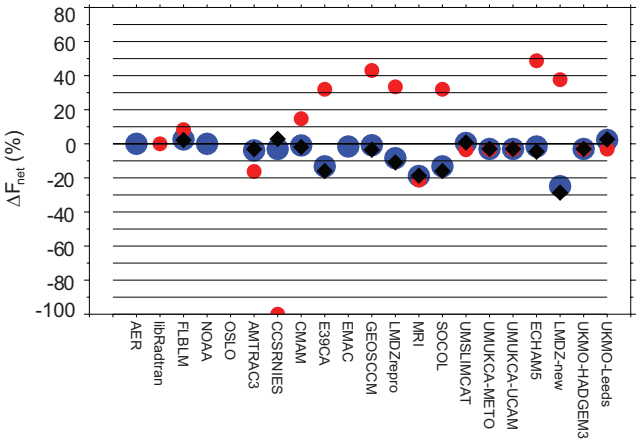

Figure 3.10: The global and diurnal mean SW (red circles), LW (blue circles) and total (black diamonds) net flux deviations of the radiative forcing due to LLGHG (case G) increase relative to the results of LBL codes (AER for LW and libRadtran for SW) at the pseudo-tropopause.

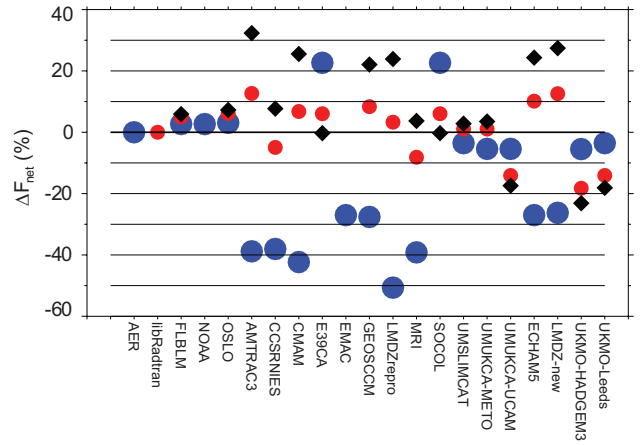

Figure 3.11: The global and diurnal mean SW (red circles), LW (blue circles) and total (black diamonds) net flux deviations of the radiative forcing due to stratospheric ozone depletion (case H) relative to the results of LBL codes (AER for LW and libRadtran for SW) at the pseudo-tropopause.

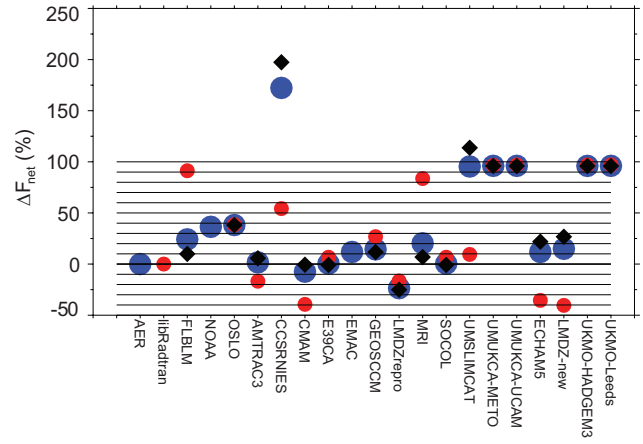

Figure 3.12: The global and diurnal mean SW (red circles), LW (blue circles) and total (black diamonds) net flux deviations of the radiative forcing due to stratospheric water vapour increase (case J) relative to the results of LBL codes (AER for LW and libRadtran for SW) at the pseudo-tropopause.

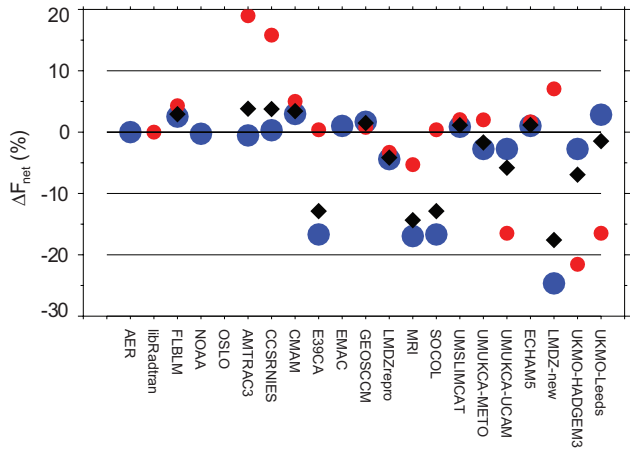

←

Figure 3.13: The global and diurnal mean SW (red circles), LW (blue circles) and total (black diamonds) net flux deviations of the radiative forcing due to LLGHG and stratospheric ozone changes (case L) relative to the results of LBL codes (AER for LW and libRadtran for SW) at the pseudo-tropopause.

Table 3.6: Globally and diurnally averaged flux differences at the pseudo-tropopause in W/m^2 for radiation models compared to reference calculations. AER is used for the LW reference and LibRadtran is used for the SW reference. The control simulation and individual forcing cases are shown. Also shown are sigma values for the total cases that are used for grading. One sigma corresponds to the maximum absolute SW difference between the LBL models and LibRadtran added to the absolute maximum LW difference between AER and the other LBL models.

All units W/m^2		Control	CO_2	CH_4	N_2O	CFC11	CFC12	Strat O_3	Trop O_3	Strat H_2O	Trop H_2O
Model	**CASE**	**A**	**B-A**	**C-A**	**D-A**	**E-A**	**F-A**	**H-A**	**I-A**	**J-A**	**K-A**
FLBLM	Lw	1.0326	0.0156	0.0005	0.0009	0.0029	0.007	0.0025	0.0013	0.0175	0.0409
FLBLM	Sw	0.8118	0.0038	0.0138	0.0004	0	0	0.017	0.0061	0.0116	0.0011
FLBLM	Tot	0.2207	0.0117	0.0132	0.0005	0.0029	0.007	0.0145	0.0074	0.0059	0.0398
NOAA	Lw	0.1995	0.0097	0.0004	0.0006	0.0026	0.006	0.0025	0.0016	0.0263	0.0073
OSLO	Lw	1.8617	0.0002	0.0033	-	-	-	0.0029	0.0007	0.0276	0.0532
OSLO	Sw	0.8783	0.0009	0.0047	-	-	-	0.0207	-	0.0049	-
OSLO	Tot	0.9834	0.0011	0.008	-	-	-	0.0178	-	0.0227	-
AMTRAC3	Lw	0.1977	0.0585	0.002	0.0025	0.0058	0.007	0.0364	0.018	0.0012	0.0183
AMTRAC3	Sw	0.1441	0.001	0.0063	0.0026	0	0	0.0429	0.0053	0.0021	0.0202
AMTRAC3	Tot	0.0535	0.0575	0.0083	0.005	0.0058	0.007	0.0793	0.0127	0.0034	0.0385
CCSRNIES	Lw	5.806	0.0425	0.0224	0.0071	0.001	0.0054	0.0357	0.0166	0.1246	0.4197
CCSRNIES	Sw	1.8613	0.0519	0.0063	0.0026	0	0	0.0168	0.0019	0.0069	0.1091
CCSRNIES	Tot	3.9447	0.0093	0.0287	0.0045	0.001	0.0054	0.0189	0.0147	0.1177	0.5289
CMAM	Lw	1.0954	0.1498	0.0084	0.0354	0.0204	0.0752	0.0397	0.0203	0.0054	0.1210
CMAM	Sw	0.0583	0.0178	0.0063	0.0026	0	0	0.0230	0.0004	0.0050	0.0001
CMAM	Tot	1.1537	0.1676	0.0147	0.0380	0.0204	0.0752	0.0626	0.0199	0.0004	0.1211
E39CA	Lw	0.5306	0.1255	0.0028	0.0165	0.0042	0.0022	0.0212	0.0196	0.0003	0.0765
E39CA	Sw	0.4057	0.0283	0.0063	0.0026	0	0	0.0205	0.003	0.0008	0.0317
E39CA	Tot	0.9363	0.1538	0.0091	0.0139	0.0042	0.0022	0.0007	0.0227	0.0005	0.0448
EMAC	Lw	0.067	0.0094	0.0379	0.0366	0.003	0.0065	0.0253	0.0108	0.0086	0.0443
GEOSCCM	Lw	5.4807	0.0296	0.0088	0.0033	0.0017	0.0067	0.0259	0.0008	0.0104	0.0317
GEOSCCM	Sw	1.8803	0.035	0.0063	0.0026	0	0	0.0283	0.0003	0.0034	0.0102
GEOSCCM	Tot	7.361	0.0646	0.015	0.0059	0.0017	0.0067	0.0542	0.0011	0.007	0.0215
LMDZrepro	Lw	9.1617	0.141	0.0199	0.0073	0.0041	0.0199	0.0475	0.0333	0.0171	0.049
LMDZrepro	Sw	0.685	0.0292	0.0063	0.0026	0	0	0.0111	0.0007	0.0021	0.0284
LMDZrepro	Tot	8.4767	0.1702	0.0262	0.0099	0.0041	0.0199	0.0586	0.034	0.015	0.0773
MRI	Lw	0.4369	0.0374	0.0117	0.049	-	-	0.0367	0.0023	0.0147	0.1326
MRI	Sw	3.91	0.0041	0.0063	0.0026	-	-	0.0276	0.0035	0.0106	0.0196
MRI	Tot	4.3469	0.0333	0.0054	0.0464	-	-	0.0091	0.0058	0.0041	0.113
SOCOL	Lw	0.5306	0.1255	0.0028	0.0165	0.0042	0.0022	0.0212	0.0196	0.0003	0.0765
SOCOL	Sw	0.4057	0.0283	0.0063	0.0026	0	0	0.0205	0.003	0.0008	0.0317
SOCOL	Tot	0.9363	0.1538	0.0091	0.0139	0.0042	0.0022	0.0007	0.0227	0.0005	0.0488
UMSLIMCAT	Lw	1.4382	0.0293	0.0181	0.0046	0.0018	0.0002	0.0033	0.0025	0.069	0.1614
UMSLIMCAT	Sw	2.0846	0.0067	0.0063	0.0026	0	0	0.0035	0.0043	0.0012	0.0639

Table 3.6 continued.

All units W/m²		Control	CO_2	CH_4	N_2O	CFC11	CFC12	Strat O_3	Trop O_3	Strat H_2O	Trop H_2O
Model	**CASE**	**A**	**B-A**	**C-A**	**D-A**	**E-A**	**F-A**	**H-A**	**I-A**	**J-A**	**K-A**
UMSLIMCAT	Tot	3.5228	0.0226	0.0118	0.0021	0.0018	0.0002	0.0069	0.0018	0.0678	0.2252
UMUKCA-METO	Lw	2.7772	0.0276	0.0023	0.0021	0.0011	0.0067	0.0051	0.001	0.0695	0.1623
UMUKCA-METO	Sw	1.7498	0.0068	0.0063	0.0026	0	0	0.0035	0.0043	0.0122	0.0103
UMUKCA-METO	Tot	1.0274	0.0344	0.0086	0.0005	0.0011	0.0067	0.0086	0.0032	0.0572	0.1725
UMUKCA-UCAM	Lw	2.7772	0.0276	0.0023	0.0021	0.0011	0.0067	0.0051	0.001	0.0695	0.1623
UMUKCA-UCAM	Sw	2.2267	0.007	0.0063	0.0026	0	0	0.0478	0.0005	0.0123	0.0115
UMUKCA-UCAM	Tot	0.5505	0.0345	0.0086	0.0005	0.0011	0.0067	0.0427	0.0016	0.0572	0.1737
ECHAM5	Lw	0.067	0.0094	0.0379	0.0366	0.003	0.0065	0.0253	0.0108	0.0086	0.0443
ECHAM5	Sw	1.3982	0.0385	0.0063	0.0026	0	0	0.0344	0.0002	0.0045	0.0369
ECHAM5	Tot	1.4652	0.0479	0.0316	0.0392	0.003	0.0065	0.0597	0.011	0.0131	0.0812
LMDZ-new	Lw	0.1507	0.0166	0.0723	0.0733	0.0251	0.0783	0.0246	0.0105	0.0108	0.0142
LMDZ-new	Sw	1.1596	0.0317	0.0063	0.0026	0	0	0.0427	0.0008	0.0051	0.0469
LMDZ-new	Tot	1.0088	0.0483	0.066	0.0707	0.0251	0.0783	0.0673	0.0098	0.0159	0.0327
UKMO-HADGEM3	Lw	2.7797	0.0277	0.0023	0.0021	0.0011	0.0067	0.0051	0.001	0.0694	0.162
UKMO-HADGEM3	Sw	0.5848	0.0069	0.0063	0.0026	0	0	0.0619	0.002	0.0123	0.0122
UKMO-HADGEM3	Tot	3.3645	0.0346	0.0086	0.0005	0.0011	0.0067	0.0568	0.003	0.0572	0.1742
UKMO-Leeds	Lw	1.471	0.0288	0.0022	0.0021	0.0011	0.0068	0.0033	0.0031	0.0695	0.142
UKMO-Leeds	Sw	2.2267	0.007	0.0063	0.0026	0	0	0.0478	0.0005	0.0123	0.0115
UKMO-Leeds	Tot	0.7557	0.0218	0.0085	0.0005	0.0011	0.0068	0.0445	0.0036	0.0572	0.1535
Sigma	Tot	2.7401	0.0194	0.0171	0.0013	0.0029	0.007	0.0236	0.0078	0.0392	0.0543

3.4.4 Heating/Cooling rates: Control experiment

In this section vertical profiles of total clear sky SW global mean heating rates (diurnally averaged) and LW cooling rates for the relevant cases are discussed. **Figure 3.14** (top panels) and **Table 3.7** show global mean SW heating rates for the control (case A) and their deviations with respect to LibRadtran. Results at three specific levels located in the lower (70 hPa), middle (15 hPa) and upper (2 hPa) stratosphere are shown in all tables of this section. The chosen levels are similar to those at which the observed temperature trends are available (Section 3.3.2). **Figure 3.15** (top panels) and **Table 3.8** show global mean LW cooling rates for case A and their deviations with respect to AER. **Tables 3.9** and **3.10** show heating and cooling rates, respectively, for a CO_2 increase. **Tables 3.11** and **3.12** show heating and cooling rates, respectively, for stratospheric ozone decrease. **Tables 3.13** and **3.14** show heating and cooling rates, respectively, for a stratospheric water vapour increase.

From Figure 3.14 it is evident that the correlations among the heating rate profiles in the stratosphere are very high, mainly due to the fact that heating rate patterns strongly depend on the gases input profiles, identical for all the models.

For case A, two sophisticated LBL heating rate calculations other than LibRadtran are available, namely OSLO and FLBLM. OSLO heating rates are in better agreement with LibRadtran below 2 hPa (see Figure 3.14 and Table 3.7). In particular, FLBLM heating rate biases at 70 hPa and 15 hPa are larger than for the OSLO model.

At 2 hPa, most of the models tend to overestimate the LibRadtran heating rates. Specifically, the biases found for LMDZ-new (15%), CMAM (9%), UMUKCA-UCAM (9%), the two UKMO models (8%) and ECHAM5 (8%) are more than a factor of two larger than the FLBLM bias (~0.18 K/day). The error at this level is consistent with an overestimation of the ozone solar heating as can be seen from Table 3.11 (case H minus case A – the instantaneous change from 10% stratospheric ozone depletion). For case H, these models report the largest negative bias at 2 hPa indicating a too large sensitivity to the ozone changes. For case A only three models present a negative bias in the heating rates larger than 0.18 K/day at this level (E39CA, LMDZrepro, SOCOL) even though they overestimate the ozone heating (Table 3.11). This under-estimation of the heating rate around the stratopause is however consistent with an under-estimation of the CO_2 heating as can be seen from Table 3.9 (case B minus case A, the instantaneous change due to CO_2 increase from 338 ppmv to 380 ppmv). However, it should be noted that the LibRadtran SW heating rates at these heights cannot be considered a good benchmark due to the differences between LBL schemes.

In the middle stratosphere (15 hPa), a better agreement is found between the models and LibRadtran, with all the models in a closer agreement with LibRadtran than FLBLM.

In the lower stratosphere (70 hPa), the biases for the majority of the models (except CCSRNIES and GEOSCCM) are also smaller than the bias found for FLBLM. In this region, the long radiative relaxation time in the lower stratosphere allows small heating and cooling rate changes to induce substantial temperature changes, therefore a heating/cooling rate bias of few tenths of a degree per day would be able to potentially warm or cool the lower stratosphere by several degrees. Specifically, for GEOSCCM the heating rate positive bias is consistent with an overestimation of the ozone absorption (see Table 3.11).

Figure 3.15 (top panels) illustrates global mean cooling rates for case A and their deviations with respect to AER. Note that the cooling rate is defined to be a positive quantity. The strong cooling peak in the upper stratosphere at about 1 hPa is due to the radiative effects of CO_2 and, by a lesser degree, O_3 and H_2O. At 1 hPa, the majority of the models under-estimate the cooling rate with a maximum negative bias of more than 3 K/day (LMDZrepro). As for the heating rates, the correlations among the cooling rate profiles in the stratosphere are high, as the cooling rates profiles strongly depend on the temperature input profiles, identical for all the models.

Table 3.8 reports the cooling rate biases for case A. Cooling rates from four LBL models are available (AER, FLBLM, NOAA and OSLO). In the lower stratosphere (70 hPa), the biases for the three LBL models with respect to AER are negative and smaller than the biases for the other models, with the exception of MRI, GEOSCCM and EMAC. The largest bias is found for CCSRNIES, partly due to an overestimation of the CO_2 and H_2O cooling (see Tables 3.10 and 3.14). At 15 hPa there is a better agreement among models and LBLs. At 2 hPa, only LMDZrepro presents a bias (17%) larger than the bias of FLBLM, consistent with a too high sensitivity to CO_2 cooling (see Table 3.10).

3.4.5 Heating/Cooling rates: Sensitivity experiments

The lower panels of Figure 3.14 report the heating rate profiles and their biases with respect to LibRadtran for case L minus case A (the instantaneous change from combined 10% stratospheric ozone depletion and 1980-2000 LLGHG changes). The LibRadtran profile shows a decreased heating rate with respect to case A, maximum above 1 hPa of ~-0.6 K/day, almost entirely due to ozone change. Between 1 hPa and 0.2 hPa the majority of the models overestimate the cooling associated with imposed ozone depletion (maximum 25%, LMDZ-new). However, it should be noted that the LBL calculations presented here cannot be considered accurate at these heights due to the strong non-LTE effects for O_3 and CO_2 solar heating in the mesosphere (*e.g.*, Fomichev, 2009).

Table 3.11 shows that in the middle and upper stratosphere almost all the models are too sensitive to imposed ozone change (negative biases) with a better agreement at 15 hPa (the maximum overestimation at this level is found for AMTRAC3) and larger biases at 2 hPa (maximum biases are found for LMDZ-new, ECHAM5 and CMAM). The maximum heating rate biases for reduced ozone at 2 hPa implies a bias in the temperature change of about 0.35 K (see Section 3.4.6). At 70 hPa AMTRAC3 and GEOSCCM are too sensitive to ozone reduction.

The second and third largest heating rate changes in the stratosphere are found for increased CO_2 from 338 to 380 ppm (case B) and 10% stratospheric water vapour increase (case J). The absorption of solar radiation by CO_2 in the near-infrared spectrum contributes to atmospheric heating of the entire atmosphere, maximising in the upper stratosphere and mesosphere (*e.g.*, Fomichev, 2009). The LibRadtran vertical profile shows positive heating rate changes in the entire atmosphere, with values ranging between +0.3% above 10 hPa and +0.6% between 100 and 10 hPa due to CO_2 increasing (not shown). The majority of contributing models overestimate the absorption of

Table 3.7: Heating rate bias of the models with respect to LibRadtran in K/day. The LibRadtran heating rate values are 0.24 K/day, 1.68 K/day and 6.6 K/day at 70 hPa, 15 hPa and 2 hPa respectively.

CASE A	70 hPa	15 hPa	2 hPa	CASE A	70 hPa	15 hPa	2 hPa
FLBLM	0.031	0.170	0.177	MRI	-0.009	-0.119	0.087
NOAA	-	-	-	SOCOL	-0.00003	-0.058	-0.200
OSLO	-0.003	0.065	-0.072	UMSLIMCAT	-0.014	-0.020	-0.013
AMTRAC3	0.003	0.146	0.255	UMUKCA-METO	-0.007	-0.004	0.011
CCSRNIES	-0.091	-0.076	0.289	UMUKCA-UCAM	-0.007	0.070	0.567
CMAM	-0.004	0.165	0.617	ECHAM5	0.015	0.101	0.471
E39CA	-0.00004	-0.058	-0.220	LMDZ-new	0.013	0.126	0.974
EMAC	-0.0127	0.0511	0.322	UKMO-HADGEM3	-0.006	0.091	0.583
GEOSCCM	0.035	0.137	0.206	UKMO-Leeds	-0.007	0.070	0.567
LMDZrepro	-0.003	-0.065	-0.226				

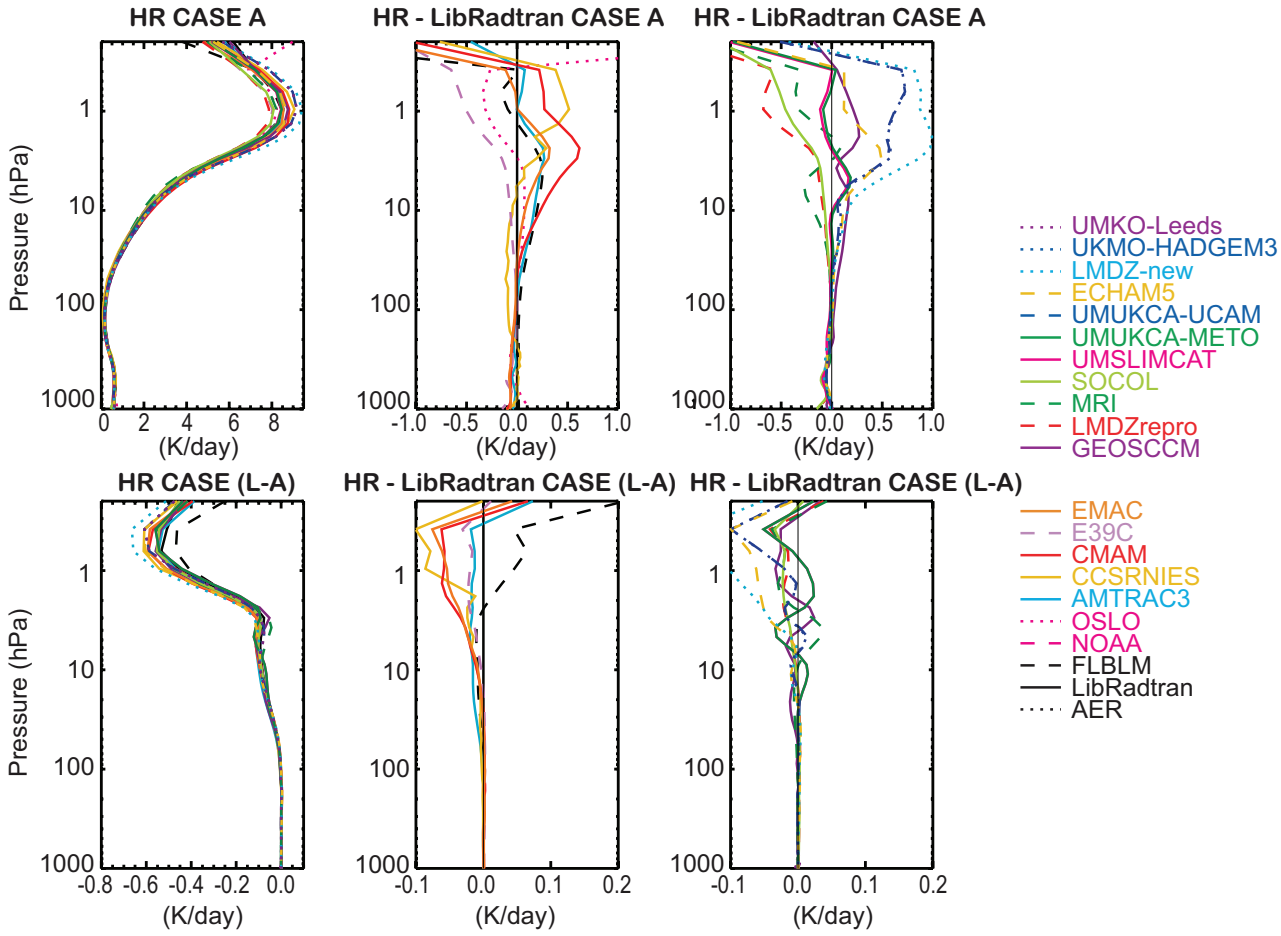

Figure 3.14: The top figures show the globally averaged shortwave heating rates for case A (control) (left) and differences in this heating rate from that calculated with the LibRadtran (middle and right). The bottom figures show the globally averaged shortwave heating rate changes for case L minus case A (the instantaneous change from combined 10% stratospheric ozone depletion and 1980-2000 LLGHG changes) (left) and differences of the same heating rate change from that calculated with the LibRadtran (middle and right).

Table 3.8: Cooling rate bias of the models with respect to AER in K/day. Results for case A (control). The AER cooling rate values are 0.3 K/day, 2.0 K/day and 6.1 K/day at 70 hPa, 15 hPa and 2 hPa respectively.

CASE A	70 hPa	15 hPa	2 hPa	CASE A	70 hPa	15 hPa	2 hPa
FLBLM	-0.009	0.112	0.454	MRI	0.011	-0.039	0.181
NOAA	-0.020	-0.011	0.092	SOCOL	-0.022	-0.217	-0.0008
OSLO	-0.017	0.026	0.199	UMSLIMCAT	-0.057	-0.133	-0.030
AMTRAC3	-0.043	-0.161	0.089	UMUKCA-METO	-0.044	-0.077	-0.442
CCSRNIES	0.141	-0.080	-0.045	UMUKCA-UCAM	-0.044	-0.077	-0.442
CMAM	-0.038	0.108	-0.451	ECHAM5	-0.025	0.026	0.089
E39CA	-0.022	-0.217	-0.0008	LMDZ-new	-0.027	0.028	0.092
EMAC	-0.012	0.118	0.402	UKMO-HADGEM3	-0.044	-0.077	-0.442
GEOSCCM	-0.018	-0.162	-0.379	UKMO-Leeds	-0.052	-0.115	0.014
LMDZrepro	-0.033	-0.015	-0.944				

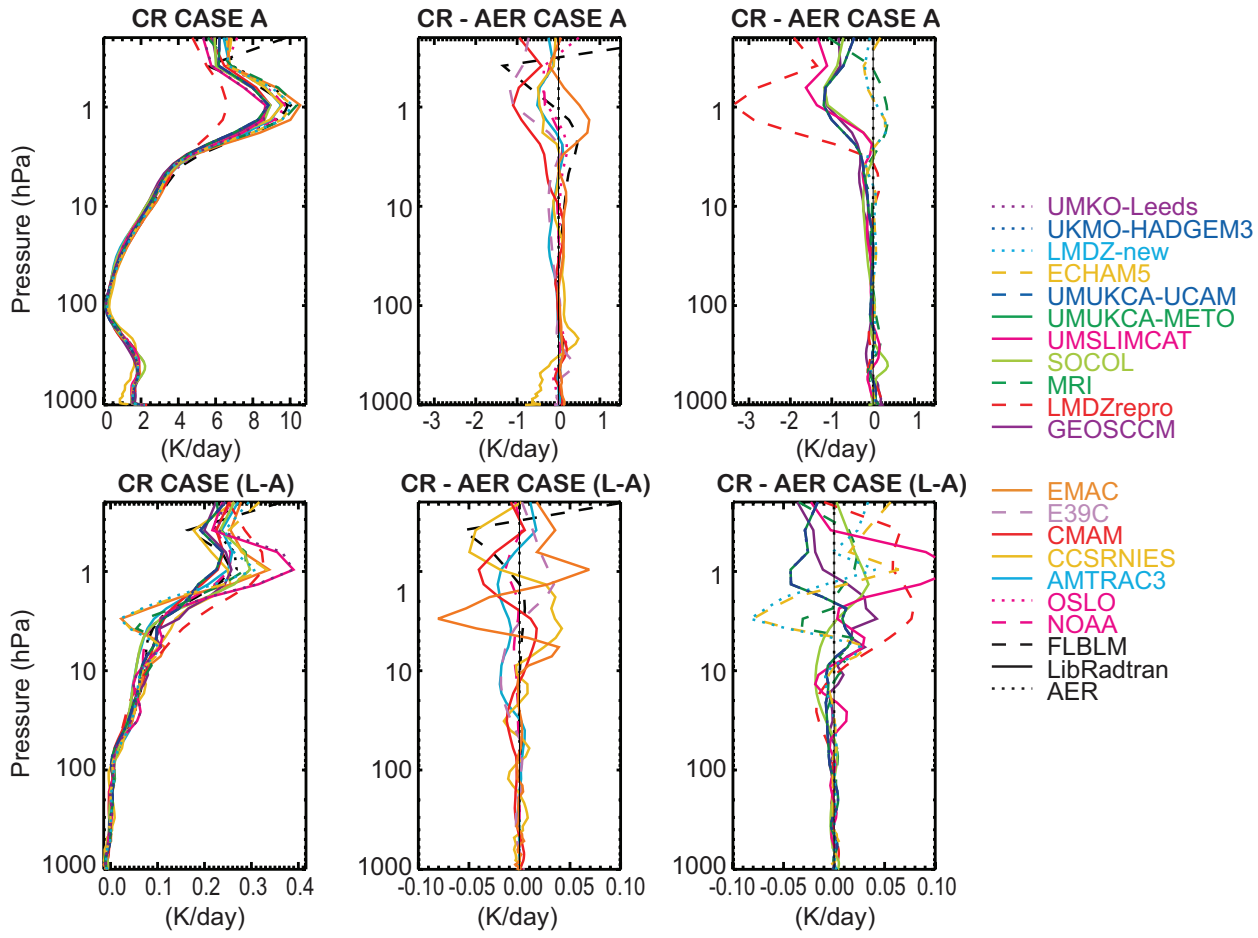

Figure 3.15: The top figures show the globally averaged longwave cooling rates for case A (control) (left) and differences in this cooling rate from that calculated with the AER model (middle and right). The bottom figures show the globally averaged longwave cooling rate changes for case L minus case A (the instantaneous change from combined 10% stratospheric ozone depletion and 1980-2005 LLGHG changes) (left) and differences of the same cooling rate change from that calculated with the AER model (middle and right).

Table 3.9: Heating rate bias of the models with respect to LibRadtran in K/day. Results are for case B minus case A (i.e., a CO_2 increase from 338 ppm to 380 ppm).

CASE B - CASE A	70 hPa	15 hPa	2 hPa	CASE B - CASE A	70 hPa	15 hPa	2 hPa
FLBLM	0.0003	0.0004	0.0004	MRI	-0.0003	-0.0009	-0.0034
NOAA	-	-	-	SOCOL	0.0030	0.0014	-0.0060
OSLO	0.0002	0.0001	0.0004	UMSLIMCAT	0.0010	0.0038	0.0104
AMTRAC3	-0.0002	0.0005	0.0033	UMUKCA-METO	0.0010	0.0037	0.0104
CCSRNIES	-0.0022	-0.0050	-0.0114	UMUKCA-UCAM	0.0010	0.0038	0.0105
CMAM	0.0021	0.0041	-0.0023	ECHAM5	0.0028	0.0034	-0.0069
E39CA	0.0030	0.0014	-0.0060	LMDZ-new	0.0026	0.0025	-0.0068
EMAC	0.0016	0.0011	-0.0078	UKMO-HADGEM3	0.0010	0.0038	0.0105
GEOSCCM	0.0013	0.0016	0.0024	UKMO-Leeds	0.0010	0.0038	0.0105
LMDZrepro	0.0031	0.0012	-0.0060				

Table 3.10: Cooling rate bias of the models with respect to AER in K/day. Results are for case B minus case A (i.e., a CO_2 increase from 338 ppm to 380 ppm).

CASE B - CASE A	70 hPa	15 hPa	2 hPa	CASE B - CASE A	70 hPa	15 hPa	2 hPa
FLBLM	0.0016	0.0010	0.0134	MRI	0.0039	-0.0080	0.0023
NOAA	0.0002	-0.0020	0.0010	SOCOL	0.0039	-0.0107	0.0252
OSLO	-0.0003	0.0004	0.0131	UMSLIMCAT	0.0006	-0.0069	0.0044
AMTRAC3	0.0008	-0.0046	0.0028	UMUKCA-METO	-0.0035	0.0015	-0.0036
CCSRNIES	0.0066	0.0055	0.0021	UMUKCA-UCAM	-0.0035	0.0015	-0.0036
CMAM	0.0004	-0.0013	0.0190	ECHAM5	-0.0012	-0.0033	-0.0579
E39CA	0.0039	-0.0107	0.0252	LMDZ-new	-0.0010	-0.0045	-0.0579
EMAC	-0.0013	0.0015	-0.0442	UKMO-HADGEM3	-0.0035	0.0015	-0.0037
GEOSCCM	0.0004	0.0049	0.0108	UKMO-Leeds	0.0006	-0.0068	0.0045
LMDZrepro	0.0004	-0.0093	0.0228				

Table 3.11: Heating rate bias of the models with respect to LibRadtran in K/day. Results are for case H minus case A (i.e., a 10% stratospheric ozone depletion).

CASE H - CASE A	70 hPa	15 hPa	2 hPa	CASE H - CASE A	70 hPa	15 hPa	2 hPa
FLBLM	-0.00123	-0.00923	-0.00046	MRI	-0.00096	-0.00411	-0.00294
NOAA	-	-	-	SOCOL	-0.00006	-0.00194	-0.01317
OSLO	-0.00082	-0.00501	0.00513	UMSLIMCAT	0.00041	0.00792	-0.00034
AMTRAC3	-0.00224	-0.01569	-0.01924	UMUKCA-METO	0.00040	0.00790	-0.00032
CCSRNIES	-0.00056	-0.00002	-0.01239	UMUKCA-UCAM	0.00064	-0.00620	-0.02986
CMAM	0.00013	-0.00919	-0.04148	ECHAM5	0.00075	-0.01238	-0.04441
E39CA	-0.00006	-0.00194	-0.01488	LMDZ-new	0.00077	-0.01144	-0.04453
EMAC	0.00002	-0.0062	-0.02905	UKMO-HADGEM3	0.00053	-0.00756	-0.03098
GEOSCCM	-0.00161	-0.00826	0.01489	UKMO-Leeds	0.00064	-0.00620	-0.02986
LMDZrepro	0.00038	-0.00172	-0.01541				

near-infrared radiation below 4 hPa (see Table 3.9). From analysis of other cases it is evident that none of the models consider absorption in the SW spectral range by LLGHG other than CO_2.

For cooling rates, the strongest cooling rate change in the stratosphere is associated with CO_2 increase (case B) and ozone depletion (case H). Figure 3.15 (lower panels) reports the cooling rate profiles and the biases with respect to AER for case L minus case A (*i.e.*, a combined effect of all LLGHG change and 10% ozone depletion). Due to combined 10% ozone depletion and LLGHG changes, an increased cooling rate of about 0.25 K/day with respect to the reference case A is found at 1 hPa for AER (Figure 3.15). The model responses deviate between 2% (AMTRAC3) and 40% (UMSLIMCAT and UMUKCA-Leeds) from this value. The FLBLM deviation is about 3% at this level.

The maximum cooling rate bias with respect to AER for imposed CO_2 increase at 70 hPa is found for CCSRNIES (Table 3.10), this value is more than a factor of four larger than the LBL bias. Also E39CA, MRI and SOCOL cooling rate biases are more than twice as large as the LBL bias. UMUKCA-METO, UMUKCA-UCAM and UKMO-HADGEM3 under-estimate the cooling rates by the same factor at this level. At 15 hPa, most of the models tend to under-estimate cooling rates due to the imposed CO_2 increase, with the maximum bias found for SOCOL and E39CA, except CCSRNIES and GEOSCCM which are too sensitive to CO_2 emission by a factor of five. At 2 hPa, EMAC, ECHAM5 and LMDZ-new present the largest negative biases in the cooling rates under-estimating the effect of CO_2 increase. These biases are of the same order of magnitude as the biases for the same models in the heating rates found for a reduction in stratospheric ozone (case H, Table 3.11).

With respect to AER the majority of the CCMVal models and other LBLs under-estimate the cooling rate decrease associated with stratospheric ozone decrease at 70 hPa and 15 hPa (Table 3.12), whereas about half of the models overestimate it at 2 hPa.

Finally, CCSRNIES significantly overestimates the cooling rate associated with stratospheric H_2O increase at 70 hPa and 15 hPa (Table 3.14), followed by UMUKCA-METO, UMUKCA-UCAM and the two UKMO models at 70 hPa and by E39CA and SOCOL at 15 hPa, whereas LMDZrepro is not sensitive enough to H_2O change at 15 hPa. CCSRNIES and the UKMO/UMUKCA based models also report too high sensitivity to H_2O change in the upper stratosphere.

A summary of heating and cooling rates biases by model is presented below. Only biases larger than the largest LBL bias are discussed.

Heating rates

EMAC slightly overestimates the heating rate in the upper stratosphere. This is consistent with an overestimation of the ozone absorption at 2 hPa.

CCSRNIES largely under-estimates heating rates at 70 hPa, whilst it overestimates them at 2 hPa (~4%), consistently with too high sensitivity of absorption of solar radiation by ozone. This model is also too sensitive to the absorption of solar radiation by H_2O at 15 hPa and 2 hPa in the infrared spectral region.

GEOSCCM overestimates heating rates at 70 hPa and 2 hPa, which is at 70 hPa consistent with an overestimation of absorption of solar radiation by ozone.

AMTRAC3, ECHAM5, LMDZ-new, CMAM, UMUKCA-UCAM, UMUKCA-HADGEM3 and the two UKMO models overestimate heating rates at 2 hPa, consistent with too large sensitivity to absorption of solar radiation by ozone. All these models, except AMTRAC3 and UMUKCA-UCAM, are not sensitive enough to absorption of solar radiation by H_2O in the infrared at 70 and 15 hPa.

E39CA, LMDZrepro and SOCOL under-estimate heating rates at 2 hPa (~3%), consistently with an underestimation of CO_2 absorption.

In general, almost all the models tend to overestimate the weak absorption of solar radiation by CO_2 in the lower and middle stratosphere, consistently with results in Section 3.4.4.

Cooling rates

CCSRNIES largely overestimates the cooling rates in the lower stratosphere (~50%). This overestimation is consistent with too high a sensitivity to emission due to CO_2 and to H_2O.

UMSLIMCAT and AMTRAC3 under-estimate the cooling rates in the lower and middle stratosphere by around ~20% and ~15%, respectively. At 15 hPa there is a competing effect of a too small sensitivity to CO_2 emission and a too high sensitivity to O_3 and/or H_2O emission.

UMUKCA-METO, UMUKCA-UCAM, UKMO-HADGEM3 and UKMO-Leeds under-estimate cooling rates in the lower stratosphere by ~ 15%. For the first three models, this under-estimation is consistent with a too small sensitivity to CO_2 emission. All four models tend to be too sensitive to both O_3 and H_2O emission.

LMDZrepro overestimates the cooling rates at 70 hPa by ~10% and at 2 hPa by ~17%, showing too large a sensitivity to O_3 emission in the lower stratosphere and to CO_2 and H_2O emission in the upper stratosphere.

CMAM under-estimates the cooling rates in the lower stratosphere by ~13%. The model biases show an increased sensitivity to O_3 emission.

SOCOL and E39CA, under-estimate the cooling rates

Table 3.12: Cooling rate bias of the models with respect to AER in K/day. Results are for case H minus case A (i.e., a 10% stratospheric ozone depletion).

CASE H - CASE A	70 hPa	15 hPa	2 hPa	CASE H - CASE A	70 hPa	15 hPa	2 hPa
FLBLM	0.0005	-0.0015	-0.0082	MRI	-0.0021	0.0063	0.0002
NOAA	-0.00003	-0.0008	-0.0015	SOCOL	-0.0013	-0.0066	-0.0052
OSLO	-0.000008	-0.0002	-0.0017	UMSLIMCAT	-0.0008	-0.0103	0.0028
AMTRAC3	0.0021	-0.0145	-0.0165	UMUKCA-METO	-0.0012	-0.0054	0.0203
CCSRNIES	-0.0004	0.0034	0.0348	UMUKCA-UCAM	-0.0012	-0.0054	0.0203
CMAM	-0.0016	0.0011	-0.0142	ECHAM5	-0.0003	-0.0001	-0.0039
E39CA	-0.0013	-0.0066	-0.0052	LMDZ-new	0.0006	-0.0002	-0.0042
EMAC	-0.0008	-0.0012	-0.0022	UKMO-HADGEM3	-0.0012	-0.0054	0.0202
GEOSCCM	-0.0015	-0.0006	0.0245	UKMO-Leeds	-0.0008	-0.0102	0.0029
LMDZrepro	-0.0033	0.0013	0.0577				

Table 3.13: Heating rate bias of the models with respect to LibRadtran in K/day. Results are for case J minus case A (i.e., a 10% stratospheric water vapour increase).

CASE J - CASE A	70 hPa	15 hPa	2 hPa	CASE J - CASE A	70 hPa	15 hPa	2 hPa
FLBLM	0.00016	0.00065	0.00285	MRI	0.00022	0.00001	0.00050
NOAA	-	-	-	SOCOL	0.00007	-0.00057	-0.00043
OSLO	-0.00005	0.00039	0.00299	UMSLIMCAT	-0.00025	-0.00057	0.00014
AMTRAC3	0.00013	-0.00029	-0.00010	UMUKCA-METO	0.00036	0.00094	0.00252
CCSRNIES	0.00015	0.00112	0.00313	UMUKCA-UCAM	0.00037	0.00094	0.00250
CMAM	-0.00036	-0.00102	-0.00047	ECHAM5	-0.00035	-0.00099	-0.00042
E39CA	0.00007	-0.00057	-0.00043	LMDZ-new	-0.00040	-0.00113	-0.00043
EMAC	-0.00036	-0.00098	-0.00042	UKMO-HADGEM3	0.00036	0.00094	0.00242
GEOSCCM	0.00010	-0.00080	-0.00051	UKMO-Leeds	0.00037	0.00094	0.00250
LMDZrepro	0.00007	-0.00058	0.00025				

Table 3.14: Cooling rate bias of the models with respect to AER in K/day. Results are for case J minus case A (i.e., a 10% stratospheric water vapour increase).

CASE J - CASE A	70 hPa	15 hPa	2 hPa	CASE J - CASE A	70 hPa	15 hPa	2 hPa
FLBLM	0.000799	0.000979	0.00204	MRI	0.003412	-0.000488	0.00023
NOAA	0.000261	-0.000408	0.00014	SOCOL	-0.001712	-0.005014	-0.00705
OSLO	0.000759	-0.000051	-0.00018	UMSLIMCAT	0.003696	0.002172	0.01682
AMTRAC3	0.000792	0.000714	0.00234	UMUKCA-METO	0.004084	0.003070	0.02056
CCSRNIES	0.009523	0.016349	0.01829	UMUKCA-UCAM	0.004084	0.003070	0.02056
CMAM	-0.000042	0.000615	-0.00076	ECHAM5	-0.000254	0.000774	0.00561
E39CA	-0.001712	-0.005014	-0.00705	LMDZ-new	-0.000316	0.001125	0.00573
EMAC	0.000188	0.001315	0.00501	UKMO-HADGEM3	0.004078	0.003060	0.02066
GEOSCCM	-0.000533	0.000485	-0.00107	UKMO-Leeds	0.004086	0.003072	0.02058
LMDZrepro	-0.001918	-0.005194	-0.01124				

in the middle stratosphere by ~10%. At 15 hPa they report a too small sensitivity to CO_2 and H_2O emission and a too high sensitivity to O_3 emission.

LMDZrepro overestimates the cooling rates at 2 hPa by ~17%, showing too large a sensitivity to CO_2 and O_3 emission at this level.

EMAC cooling rate response to CO_2 increase (case B) substantially deviates from LBL model results above 10 hPa. The same behaviour is also observed for ECHAM5 and LMDZ-new models which exploit similar LW codes.

Table 3.15 shows total (SW+LW) heating rates and sigmas used for the three cases used for grading, analysed at the three levels. One sigma corresponds to the maximum absolute SW difference between LBL models and LibRadtran added to the absolute maximum LW difference between AER and the other LBL models. See Section 3.6 for grading discussion.

3.4.6 Radiation scheme errors and model temperature biases

In this section the assessment of the heating and cooling rates from Section 3.4 is applied to the analysis of the stratospheric temperatures biases simulated by the CCMs. Biases in the global mean temperature climatology (reported in Section 3.3.1) are compared with the temperature errors arising both from the inaccuracy of the radiative heating rate calculations and from the biases in simulated ozone and water vapour mixing ratios (see Section 3.3.1).

The potential errors in the temperature simulations from errors in heating and cooling rates are estimated by converting the results from the offline heating and cooling rate calculations for reference case A to temperature using pre-calculated relaxation times. Relaxation times represent the thermal inertia due to radiative transfer and

Table 3.15: Total (SW+LW) heating rates and sigmas used for the three cases used for grading, analysed at the three levels: 70, 15 and 2 hPa. One sigma corresponds to the maximum absolute SW difference between LBL models and LibRadtran added to the absolute maximum LW difference between AER and the other LBL models.

All units K/day	Control (CASE A)			CO2 increase (CASE B-A)			10% stratospheric ozone depletion		
Model	**70 hPa**	**15 hPa**	**2 hPa**	**70 hPa**	**15 hPa**	**2 hPa**	**70 hPa**	**15 hPa**	**2 hPa**
FLBLM	0.04	0.058	-0.277	-0.0013	-0.0006	-0.013	-0.00173	-0.00773	0.00774
OSLO	0.014	0.039	-0.271	0.0005	-0.0003	-0.0127	-0.00081124	-0.00481	0.00683
AMTRAC3	0.046	0.307	0.166	-0.001	0.0051	0.0005	-0.00434	-0.00119	-0.00274
CCSRNIES	-0.232	0.004	0.334	-0.0088	-0.0105	-0.0135	-0.00016	-0.00342	-0.04719
CMAM	0.034	0.057	1.068	0.0017	0.0054	-0.0213	0.00173	-0.01029	-0.02728
E39CA	0.019	0.158	-0.218	-0.0009	0.0122	-0.0312	0.00124	0.00466	-0.00928
EMAC	-0.0007	-0.0669	-0.08	0.0029	-0.0004	0.0364	0.00082	-0.005	-0.02685
GEOSCCM	0.053	0.299	0.585	0.0009	-0.0033	-0.0084	-0.00011	-0.00766	-0.00961
LMDZrepro	0.03	-0.05	0.718	0.0027	0.0105	-0.0288	0.00368	-0.00302	-0.07311
MRI	-0.02	-0.08	-0.094	-0.0042	0.0071	-0.0057	0.00114	-0.01041	-0.00314
SOCOL	0.018965	0.158	-0.198	-0.0009	0.0122	-0.0312	0.00124	0.00466	-0.00757
UMSLIMCAT	0.043	0.113	0.017	0.0004	0.0107	0.006	0.00121	0.01822	-0.00314
UMUKCA-METO	0.037	0.073	0.453	0.0045	0.0022	0.014	0.0016	0.0133	-0.02062
UMUKCA-UCAM	0.037	0.147	1.009	0.0045	0.0023	0.0141	0.00184	-0.0008	-0.05016
ECHAM5	0.04	0.075	0.382	0.004	0.0067	0.051	0.00105	-0.01228	-0.04051
LMDZ-new	0.04	0.098	0.882	0.0036	0.007	0.0511	0.00017	-0.01124	-0.04033
UKMO-HADGEM3	0.038	0.168	1.025	0.0045	0.0023	0.0142	0.00173	-0.00216	-0.05118
UKMO-Leeds	0.045	0.185	0.553	0.0004	0.0106	0.006	0.00144	0.004	-0.03276
Sigmas	0.05	0.18	0.631	0.0019	0.0024	0.0139	0.00183	0.01073	0.01333

are estimated from the cooling rate response to a constant (with height) 1 K temperature change using the correlated k-distribution scheme by Li and Barker (2004). At three considered levels in the lower (70 hPa), middle (15 hPa) and upper (2 hPa) stratosphere, the estimated global mean relaxation times are 180, 25 and 8 days respectively.

The contribution from the ozone and water vapour biases is estimated using biases from Section 3.3.1 to scale the radiative response to the stratospheric ozone depletion and water vapour increase (cases H and J) simulated by the participating models. The obtained errors in the heating and cooling rates associated with the model's ozone and water vapor biases are also converted to an equivalent temperature bias using the relaxation time. This procedure provides temperature errors for all participating models related both to the errors in the LW and SW radiation codes and to the errors in the simulated ozone and water vapour fields.

The analysis has been carried out for the upper, middle and lower stratosphere (pressure levels 2, 15 and 70 hPa) and the conclusions drawn in this section generally confirm the qualitative assessment of the upper stratospheric model performance in Section 3.3.1. The results for the upper stratosphere (2 hPa) are shown in **Figure 3.16**. At this level the total temperature errors derived from the inaccuracy of the radiation schemes and the biases in ozone and water vapour abundances are very close to the temperature biases simulated by the CCMs for most of the participating models (black diamonds and black circles, respectively). For AMTRAC3 the small positive temperature bias is explained by overestimated solar heating rates. The large temperature bias for CCSRNIES results from under-estimated longwave cooling rates, overestimated solar heating rates, and a negative bias in the simulated water vapour mixing ratio, with all three factors contributing about equally. The large warm bias for CMAM is explained both by overestimation of solar heating rates and under-estimation of cooling rates. The small temperature bias for EMAC is due to its overestimated cooling rates. For GEOSCCM the warm bias is produced by overestimated heating rates and under-estimated cooling rates and is partially compensated by under-estimated ozone mixing ratios. The very large temperature bias for LMDZrepro is dominated by a massive under-estimation of the cooling rates. The negative temperature bias for MRI is mainly due to slightly overestimated cooling rates, while the same sized bias in SOCOL is primarily due to under-estimated solar heating rates and a negative bias in the ozone mixing ratio. UMSLIMCAT has only a very small cold bias, for which a small under-estimation of the cooling rates is compensated by the cumulative effects of small errors in solar heating and water vapour and ozone mixing ratios. Warm biases in UMUKCA-METO and UMUKCA-UCAM result primarily from under-estimated cooling rates, although under-estimated water vapour mixing ratios for UMUKCA-METO and overestimated solar heating rates and under-estimated ozone mixing ratios for UMUKCA-UCAM also contribute significantly.

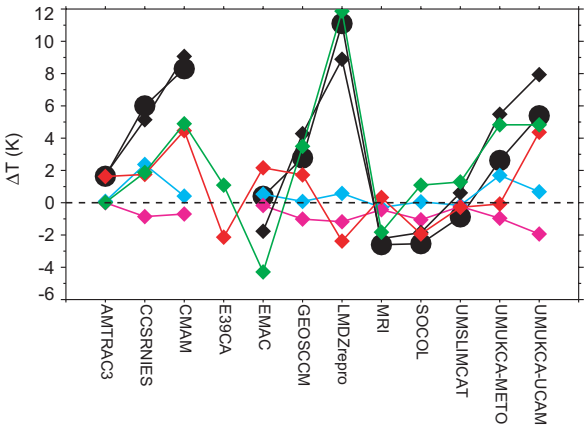

Figure 3.16: The bias in the simulated global mean temperature at 2 hPa from Section 3.3 (black circles) and the estimated contributions of CCM biases in: ozone climatology (pink diamonds); water vapour climatology (light blue diamonds); and longwave/shortwave heating rates calculations (green/red diamonds). The total CCM bias is represented by black diamonds. See text for details.

Four models were singled out in the analysis of simulated temperature climatologies in Section 3.3.1 as likely to have deficiencies in their radiation schemes in the upper stratosphere: CCSRNIES, CMAM, CNRM-ACM and LMDZrepro. While CNRM-ACM is not analysed here, the present analysis confirms the qualitative assessment made in Section 3.3.1 for the other three models.

In the middle stratosphere (15 hPa) and in the lower stratosphere (70 hPa) the temperature biases and estimated errors (not shown) are generally well correlated but significant discrepancies between the two values exist, making a similar analysis less useful for these heights. This is probably due to a number of reasons. First, using relaxation time for the conversion heating rate to temperature is a rough approach which works better in the vicinity of the stratopause than in the middle and lower stratosphere where the relaxation time depends more strongly on the shape of the perturbation and has a strong latitudinal dependence. Second, the effect of errors in O_3 and H_2O mixing ratios has been estimated based on the local biases. However, non-locality plays an important role in the middle and lower stratosphere for both solar heating and longwave cooling rate calculations. Third, the temperature biases reported in Section 3.3.1 are based on the annually averaged global mean climatology, whereas heating rates used to estimate errors are global values based on calculations at five latitudes for January conditions. And finally, the effect of clouds and volcanic aerosol which is important in the

lower and middle stratosphere, was not evaluated in the framework of this exercise.

3.5 Solar signal in CCMs

The incident solar radiation at the top of Earth' atmosphere varies on different time scales. Observational studies, *e.g.*, Randel *et al*. (2009), found a statistically significant decadal signal in annual mean upper stratospheric temperature of up to 1 K, associated with the 11-year solar activity cycle. While the total solar irradiance (TSI), *i.e.*, the spectrally integrated solar irradiance at the top of Earth's atmosphere, varies only by about 0.1% over the 11-year cycle, larger variations occur in the ultraviolet (UV) part of the spectrum, reaching several percent in the ozone absorption bands that are responsible for the SW heating of the stratosphere. However, given the much lower intensity in the UV spectral region compared to the visible (VIS) and near-infrared (IR) parts of the solar spectrum, and because of the historical focus of numerical global modelling on the troposphere where absorption of solar UV radiation by ozone plays only a very minor role, SW radiation codes in GCMs and CCMs do not consider the solar irradiance for the wavelengths shorter than ~250 nm and quite often exploit broad-band parameterisations using TSI as an input variable. Depending on the radiation scheme, fractions of TSI are then used to calculate solar fluxes and heating rates in one or two SW absorption bands from the top of the atmosphere to the surface. More sophisticated SW radiation codes designed for applications to the middle atmosphere usually consider extended spectral range and include more spectral bands in the UV/VIS. Egorova *et al*. (2004) and Nissen *et al*. (2007) compared the performance of SW radiation codes with different spectral resolution and showed that the observed solar temperature signal in the stratosphere can only be reproduced in models that allow for the effects of spectral variations between solar minimum and maximum.

In this section we will address the following questions:

1. How sensitive are the CCM SW radiation codes to changes in solar irradiance and ozone?
2. How well is the 11-year radiative solar signature reproduced by the participating SW radiation codes in comparison with reference LBL codes?
3. Can the grade of the simulated solar signature in temperature in the REF-B1 simulations, discussed in Chapter 8 of this report, be explained in terms of the characteristics of the SW radiation codes?

3.5.1 Experimental Setup

Heating rate differences between the minimum and maximum phases of the 11-year solar cycle have been calculated in stand-alone versions of the CCM shortwave radiation parameterisations and in LBL models for prescribed spectral flux and solar induced ozone differences between the minimum and maximum phases of the 11-year solar cycle.

The spectral solar irradiance (SSI) and TSI data to be used in this comparison are based on the method described in Lean *et al*. (2005). Extra-terrestrial spectral solar irradiance for the spectral range 120 – 100,000 nm were provided with a spectral resolution ranging from 1 to 50 nm as well as the spectral integral over all wavelengths, *i.e.*, TSI. The monthly mean solar irradiance of September 1986 and November 1989 has been selected for solar minimum and solar maximum conditions, respectively. For mean solar conditions average data were derived from the period 1950 to 2006. Depending on the individual SW radiation codes, the modelling groups were requested to either use the suggested TSI for solar minimum and maximum conditions, or to integrate the provided high resolution spectral irradiances to match the broader spectral intervals of their own SW radiation codes and to adapt the total solar irradiance to be consistent with the integral over all intervals. To study the effect of solar induced ozone variations on heating rates, experiments with mean solar irradiance and prescribed ozone changes between solar minimum and

Table 3.16: Experimental setup for offline solar variability simulations.

Experiment	Solar irradiance	Ozone
A	mean	1980 climatology
O	max	1980 climatology
P	min	1980 climatology
R	mean	max
S	mean	min

Table 3.17: Participating offline SW radiation codes and ways of prescribing solar variability.

CCM	TSI	Spectral
CCSRNIES		√
CMAM		√
ECHAM4	√	
ECHAM5		√
EMAC		√
LMDZrepro	√	
SOCOL		√
UMSLIMCAT		√
UMUKCA-METO	√	
UMUKCA-UCAM	√	

maximum were carried out. The ozone changes have been derived from 2-dimensional, photochemical model calculations (Haigh, 1994) to ensure smooth distributions of the changes.

Further settings of the experiments were identical to the 1980 control simulation (case A, Table 3.4). **Table 3.16** gives an overview of the recommended experiments.

The participating CCM SW radiation codes and the provided SW radiative heating rates are summarized in **Table 3.17**. Further it is indicated whether the radiation codes are forced with TSI or spectral irradiance data. More details of the radiation codes including references can be found in Chapter 2.

The results of the offline calculations have been evaluated against reference calculations from the LBL radiation code LibRadtran (Meyer and Kylling, 2005).

3.5.2 Sensitivity of the solar signal to spectral resolution

Figure 3.17 shows global mean profiles of the differences in SW heating rates between solar minimum and maximum in January. In the left panel only solar irradiance variations are taken into account and in the middle panel the effects of prescribed solar induced ozone changes only. The right panel shows the total effects of solar irradiance and prescribed solar induced ozone changes between solar minimum and maximum. The largest response to 11-year solar irradiance changes (experiments O-P, left panel) occurs in the stratopause region with global mean heating rate changes from solar minimum to maximum of about 0.12 K/day in the LibRadtran reference model (black line). The results of the CCM radiation schemes can be grouped into three categories: a) schemes that closely follow the reference heating rate change profile, *i.e.*, CMAM, EMAC and CCSRNIES, and with some minor deviations SOCOL, b) two schemes that reproduce about half of the reference heating rate differences (ECHAM5 and UMSLIMCAT) and c) schemes that have an almost negligible radiative response to solar irradiance changes of less 0.02 K/day, like ECHAM4, LMDZrepro, UMUKCA-METO, and UMUKCA-UCAM.

Differences between the three groups can be explained by the spectral resolution of the prescribed solar irradiance change between solar minimum and maximum. With 44 spectral intervals between 121 and 683 nm the EMAC scheme reproduces the reference profile over the whole stratosphere very well; similarly the CMAM code with 8 bands between 121 and 305.5 nm and only 3 bands for ozone absorption between 206 and 305.5 nm. SOCOL (4 spectral intervals between 120 and 680 nm) overestimates the maximum SW heating rate difference in the lower mesosphere by about 10%, associated with an under-estimation in the lower stratosphere. In contrast, the SW radiation codes in LMDZrepro, UMUKCA-METO, UMUKCA-UCAM, and ECHAM4 that are driven by TSI changes between solar minimum and maximum only, are not able to capture the magnitude of the SW heating rate changes between solar minimum and maximum.

The SW radiation scheme of the Unified Model (UM) model series can also be driven by spectral irradiance changes, as was done for example in the REF-B1 simulation of UMSLIMCAT. This allows for a direct assessment of the effect of spectral irradiance versus TSI input data. As seen in Figure 3.17 (left panel), the SW heating rate response of the spectrally forced offline calculation with UMSLIMCAT is stronger than in the TSI forced UMUKCA-METO and UMUKCA–UCAM models. However with a SW heating rate difference of ~0.07 K/day, UMSLIMCAT reproduces only about 50% of the LBL model result. A similar result to that of UMSLIMCAT is obtained for ECHAM5. The ECHAM5 offline radiation code was included into this comparison to investigate the effect of adding two bands in the UV to the single UV/VIS absorption band used in the ECHAM4 code (Cagnazzo *et al.*, 2007). Although with the additional absorption bands (185-690 nm) the full spectral range of ozone absorption is resolved, only 50% of the heating rate differences between solar minimum and maximum can be simulated.

The global mean SW heating rate response to prescribed solar induced ozone changes (experiments R-S, middle panel of Figure 3.17) in the reference model reaches about 0.07 K/day from solar minimum to maximum, that is approximately 65% of the response to the solar irradiance variations. The strongest response occurs in the upper stratosphere, about 10 km lower than the strongest response to irradiance changes. This behaviour is qualitatively well reproduced by the different CCM radiation codes. Deviations from the LBL code are much smaller than for the irradiance changes, as mean solar irradiance was prescribed to isolate the clean 'ozone effect'. Differences between the models occur due to the band width adopted and generally correspond to the differences encountered in case A. Note that the 'ozone effect' exceeds the effect of solar irradiance variations below 10 hPa emphasising the importance of considering the feedback of changes in ozone photochemistry during a solar cycle on the SW radiation budget.

The total SW heating rate change between solar minimum and maximum, *i.e.*, due to both solar irradiance changes and the solar induced ozone changes, (right panel in Figure 3.17) clearly illustrates that those CCM SW radiation codes that use only TSI variations under-estimate the solar radiative signal by about 50%.

The response to solar variability obtained with the CCM SW radiation codes in offline mode is generally consistent with the solar response in the transient REF-B1 simulations discussed in Chapter 8. The REF-B1 solar heating rate differences for those models, which also pro-

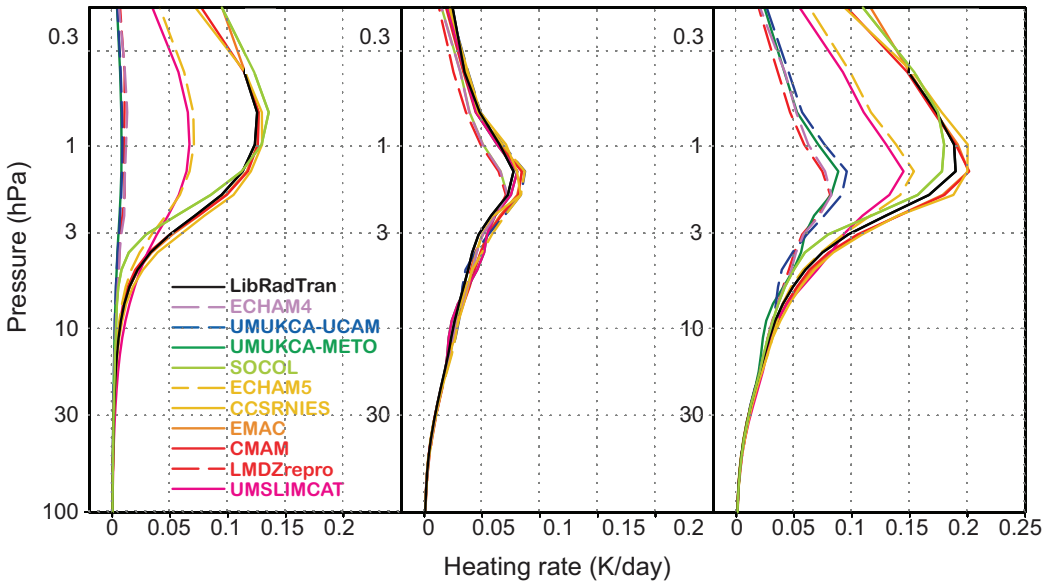

Figure 3.17: Global mean, shortwave heating rate differences between minimum and maximum of the 11-year solar cycle in January (K/d), calculated offline in CCM radiation schemes and one reference LBL model. Left panel: Radiative response to prescribed solar irradiance change (experiments O-P, Table 3.16), middle panel: radiative response to solar induced ozone change (experiments R-S, Table 3.16), right panel: total radiative response (experiments (O-P)+(R-S), Table 3.16).

vided off-line heating rates (CCSRNIES, CMAM, EMAC, and LMDZrepro) range between 0.07 and 0.17 K per day per 100 units of the F10.7cm solar flux around the tropical stratopause (Figure 8.12). By multiplying these values by a factor 1.3 we obtain an estimate of the SW heating rate differences between solar minimum and maximum that can be compared with the offline calculations. There is good agreement between online and offline calculated heating rate differences for the four CCMs (not shown). For example, we find an annual mean tropical heating rate difference of 0.20 K per day in the REF-B1 run of CMAM and a heating rate difference of 0.22 K per day at the equator in January from the CMAM offline code.

In Chapter 8, the temperature response to decadal solar forcing in the CCMs was derived by a multiple linear regression analysis (Figure 8.11). The strongest solar temperature signal is found consistently in the tropical upper stratosphere/lower mesosphere, indicating that the direct mechanism of heating by absorption of enhanced UV radiation at solar maximum is well captured by the spectrally resolving SW radiation schemes. The reduced decadal temperature signal in LMDZrepro can be explained by the under-estimation of the spectral solar forcing that was identified in the offline calculations. However, while the responses to solar irradiance changes in the spectrally resolving radiation codes of CCSRNIES, CMAM, EMAC, and SOCOL are close to each other (Figure 3.17, left panel), the solar temperature responses in the corresponding REF-B1 simulations of these models show a considerable spread in the upper stratosphere and mesosphere (Figure 8.11a), which cannot be explained by a direct radiative effect alone. Similarly, indirect dynamical processes seem to contribute to the strong solar response of mesospheric temperature in the UMSLIMCAT REF-B1 simulation, as the offline calculation shows that its SW radiation code underestimates the heating rate response to UV-variations.

3.6 Summary

In this section, as in other chapters, we employ the concepts of metrics and grades to help synthesize the discussions of the preceding sections. A metric can been seen as a way for assessing a model and comparing it to an objective benchmark. For example we compare a model's globally averaged temperature to an observed climatological mean. In this case the metric would be temperature difference, and the benchmark given as the observed climatological mean temperature. A grading is then applied to this temperature difference according to how big a difference is deemed acceptable without down-grading the model performance. For our example, we compare the model temperature difference to the observed interannual variability in temperature, and say that a model with an error smaller than the interannual variability is performing well, and assign the model a "good" grade.

We adopt the above approach in a quantitative way. Each CCM is graded between zero and one, with a grade of one representing a "perfect" result and a grade of zero representing no skill. The gradings are based on a standard

deviation approach where, nominally, one sigma (σ) away from the reference diagnostic reduces the grade by 0.33. For deviation X from the reference diagnostic, a grade (G) is given by

$$G = 1 - 0.33\, X/\sigma, \qquad (3.1)$$

Therefore, three or more sigmas away from the reference diagnostic would give a grade of zero. For most metrics, a sigma value could not be calculated from statistics so the choice of sigma values and grading has been somewhat subjective. Table 3.1 summarizes the metrics and gradings used to evaluate each processes. **Table 3.18** gives details of each grading used and tables in the chapter that give the diagnostics and sigma values that are used to calculate the grades for each process.

Three sets of gradings are shown in Figures 3.18 to 3.21. These refer to temperature based diagnostics (**Figure 3.18**), flux diagnostics (**Figure 3.19**) and heating rate diagnostics (**Figure 3.20**). Sigma values used are based on interannual variability measures for temperature trend metrics. For other metrics sigmas are based on the maximum difference between CCMs and either reference analyses or reference calculations. Therefore, a model grade above 0.66 is as good as can be expected with current knowledge. We class grades as 0.66 or higher "good", grades between 0.33 and 0.66 as "adequate" and grades below 0.33 as "poor". Note that many caveats exist in grade representation and these grades should not be seen as definitive or over interpreted. A different choice of diagnostic, reference model and/or sigma can lead to different answers. We have tried to be pragmatic with these choices, picking metrics that we believe to be most relevant to the CCM community, although a degree of subjectivity will still exist.

By deriving sigma values from differences between reference calculations a poor grading does not necessarily mean a large source of model error. Take, for example, the CO_2 and stratospheric water vapour forcing grades in Figure 3.19. The stratospheric water vapour forcing has errors of over 100% between models (Figure 3.12), yet model grades are adequate or good. Whereas, the error in CO_2 forcing is estimated to be within 20% (Figure 3.9) yet several CCMs are given a poor grade. This, perhaps unintuitive, grading results from the CO_2 forcing being much better constrained between the reference sets of calculations, compared to the reference calculations for stratospheric water vapour. Our choice of metric can therefore be seen as an indictor of how close a model is to "state of the art" rather than how accurate a model is.

General grading features are discussed here. Individual model grades and performance and summarized in Section 3.6.1.

Many CCMs have poor representation of lower stratospheric temperatures yet are able to produce a good simulation of temperature trends throughout the stratosphere (Figure 3.18). This likely is, in part, due to temperature changes depending largely on carbon dioxide and ozone changes, whereas many other factors such as clouds can affect temperature climatologies in the lower stratosphere. The multi-model mean has a higher grade than all but one model (WACCM) which indicates the value of multi-model studies.

CO_2 and N_2O forcings are generally less well modelled by CCMs than by LBLs, so CCMs typically have a poor grader for these forcings, indicating potential areas for radiation scheme improvement (Figure 3.19). When gradings are combined with knowledge of radiation scheme errors (see above), a good grade for stratospheric water vapour changes suggests that at least some of the sets of reference calculations should be improved.

Stratospheric heating rate based metrics for the climatology, CO_2 increases and ozone depletion are shown in Figure 3.20. These grades are generally good across CCMs, meaning that CCMs should be able to provide good estimates of temperature change. Hence these grades corroborate the temperature trend based grade results in Figure 3.18.

The aim of Section 3.5 was to validate the ability of the CCM SW radiation codes to reproduce the radiative effects of decadal solar variability. Therefore, the basis for allotting grades to the different SW radiation codes is their response or sensitivity to solar irradiance changes that vary increasingly towards shorter wavelengths between solar minimum and maximum, reaching several percent in the UV. The comparison described here clearly revealed that only CCM radiation codes that are designed to take prescribed spectral irradiance data into account are able to reproduce the magnitude and vertical profile shape of the heating rate differences between solar minimum and maximum (Figure 3.17, left panel). These models (CCSRNIES, CMAM, EMAC, and SOCOL) simulate the reference heating rate difference profile within a few percent and are therefore graded as 0.9. Another class of models fails to reproduce the solar signal in SW heating rates due to their neglect of spectral irradiance changes. These models (ECHAM4, LMDZrepro, UMUKCA-METO, and UMUKCA-UCAM) are graded as 0.1. Two models (ECHAM5 and UMSLIMCAT) are able to alleviate the bias to some extent by considering spectral irradiance changes in a simplified way. They reproduce about half the variability in SW heating rates, and are therefore graded as 0.5.

This grading also applies to the total effects of solar variability (Figure 3.17, right panel) including the effects of solar induced ozone changes, as the heating rate changes due to prescribed solar induced ozone changes (Figure 3.17, middle panel), are well captured by most models. As the outcome of this inter-comparison clearly suggests three categories of SW radiation codes, we abstain from a more

Table 3.18: A summary of the metrics and gradings used to evaluate each processes.

Process	Metric	Metric sigma basis	Grading basis
Stratospheric temperatures	Comparing 1980-1999 climatological global mean temperature profiles	Maximum difference between ERA 40 and either UKMO or NCEP analysis. Evaluated at 70 hPa, 15 hPa and 2 hPa	See Table 3.2
Stratospheric temperature change	Comparing 1980-1999 global mean temperature trends	MSU/SSU trend uncertainty (95% confidence interval). Evaluated at 70 hPa, 15 hPa and 2 hPa	See Table 3.3
Radiative fluxes	Comparing global mean total (SW+LW) climatological fluxes in offline radiation schemes with LBL models	Maximum difference between sophisticated radiation models for globally annually averaged total (SW+LW). Evaluated at the tropopause	See Table 3.6
Radiative forcing	Comparing global mean instantaneous total forcings (SW+LW) in offline radiation schemes for a variety of atmospheric composition changes with LBL models	Maximum difference between sophisticated radiation models for globally annually averaged total (SW+LW). Evaluated at the tropopause	See Table 3.6
Stratospheric heating/cooling	Comparing global mean total (SW+LW) climatological heating rates in offline radiation schemes with LBL models	Maximum difference between sophisticated radiation models for globally annually averaged total (SW+LW). Evaluated at 70 hPa, 15 hPa and 2 hPa	See Table 3.15
Changes in stratospheric heating/cooling	Comparing changes in globally averaged total (SW+LW) heating rates in offline radiation schemes with LBL models	Maximum difference between sophisticated radiation models for globally annually averaged total (SW+LW). Evaluated at 70 hPa, 15 hPa and 2 hPa	See Table 3.15
Solar variability	Comparing globally averaged SW heating rates in offline radiation schemes with prescribed solar spectrum variations and ozone change	Whether or not radiation code reproduces sophisticated model signal. A subjective grade based on how similar their signal is to LibRadtran results	See Figure 3.17

detailed grading.

Throughout the chapter we have tried to explain differences between CCMs. However, in many instances appropriate diagnostics were not available and interpretation is lacking, so a full assessment of differences has not been possible.

3.6.1 Summary by model

We class grades as 0.66 or higher "good", grades between 0.33 and 0.66 as "adequate" and grades below 0.33 as "poor". We employ this standard terminology to the model summaries below. For English clarity respective adverb forms of "well", "adequately" and "poorly" are also employed,

AMTRAC3: This CCM has an adequate representation of climatological global mean temperatures in the lower and middle stratosphere, and a good representation of temperatures in the upper stratosphere. Global mean temperature trends throughout the stratosphere are well reproduced. Climatological total radiative flux at the tropopause is well modelled. Radiative forcings at the tropopause are well modelled for water vapour changes, both in the stratosphere and troposphere, and for CH_4. CFC forcings and tropospheric O_3 forcings are adequately modelled. CO_2, stratospheric O_3 and N_2O forcings are poorly modelled. Climatological heating rates and their change from CO_2 and stratospheric O_3 perturbations are either adequate or

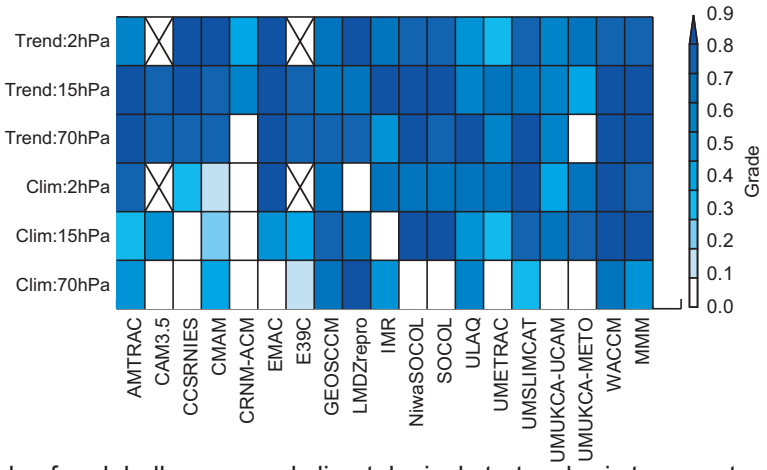

Figure 3.18: CCM grades for globally averaged climatological stratospheric temperatures and their trend. See Table 3.18 for details.

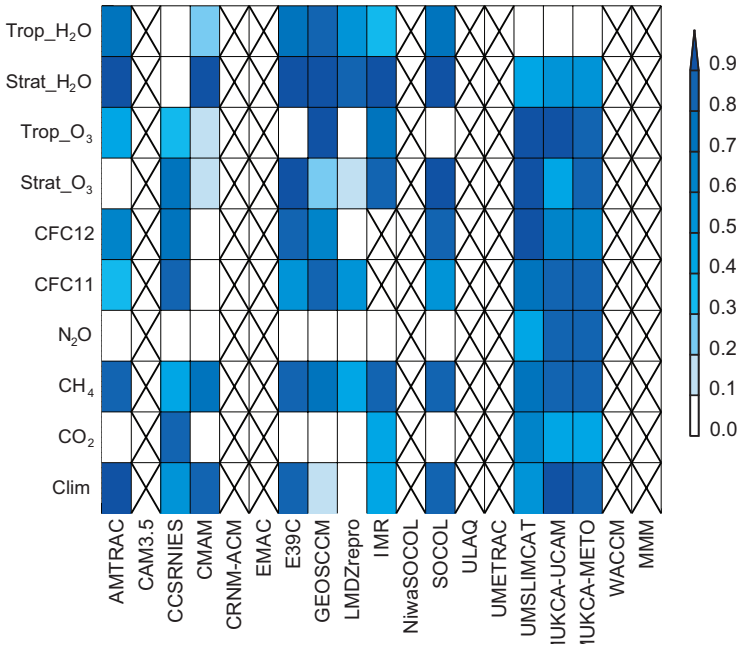

Figure 3.19: CCM grades for globally averaged fluxes at the 200 hPa tropopause and their change (radiative forcing). See Table 3.18 for details.

better. The CCM's representation of solar variability is not assessed.

CAM3.5: This CCM has a low model lid so upper stratospheric levels were not assessed. This CCM has an adequate representation of climatological global mean temperatures in the middle stratosphere, and a poor representation of temperatures in the lower stratosphere. Global mean temperature trends throughout the CCM's stratosphere are well reproduced. The CCM's representation of fluxes, heating rates and solar variability is not assessed.

CCSRNIES: This CCM has an adequate representation of climatological global mean temperatures in the upper stratosphere, and a poor representation of temperatures in the lower and middle stratosphere. Global mean temperature trends throughout the stratosphere are well reproduced. Climatological total radiative flux at the tropopause is adequately modelled. CO_2, stratospheric O_3 and CFC forcings are well modelled. CH_4, and tropospheric ozone forcings are adequately modelled. Radiative forcings at the tropopause are poorly modelled for water vapour changes, both in the stratosphere and troposphere, and for N_2O. Climatological heating rates are well represented, except in the lower stratosphere which is poorly represented. Changes in heating rates are well modelled for ozone in the lower and middle stratosphere and for CO_2 in the upper stratosphere. Middle and lower stratospheric heating

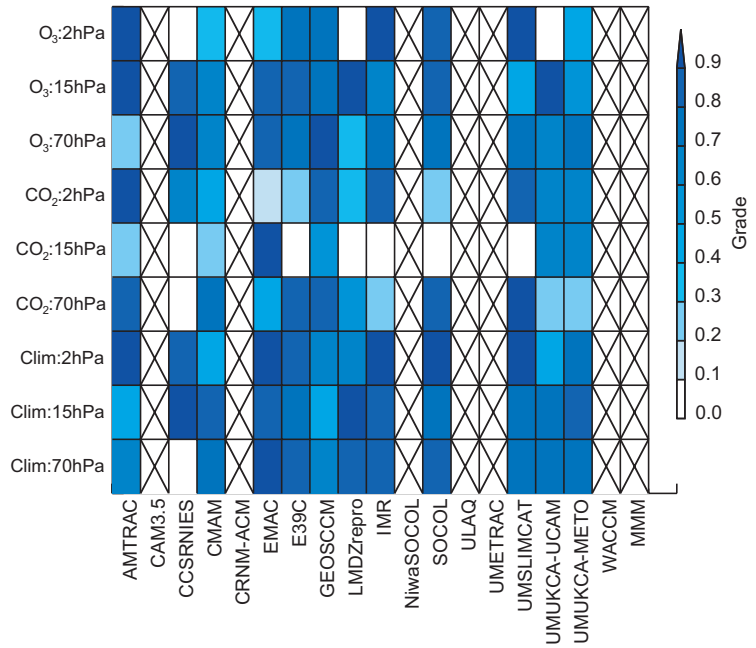

Figure 3.20: CCM grades for globally averaged climatological stratospheric heating rates and their changes. See Table 3.18 for details.

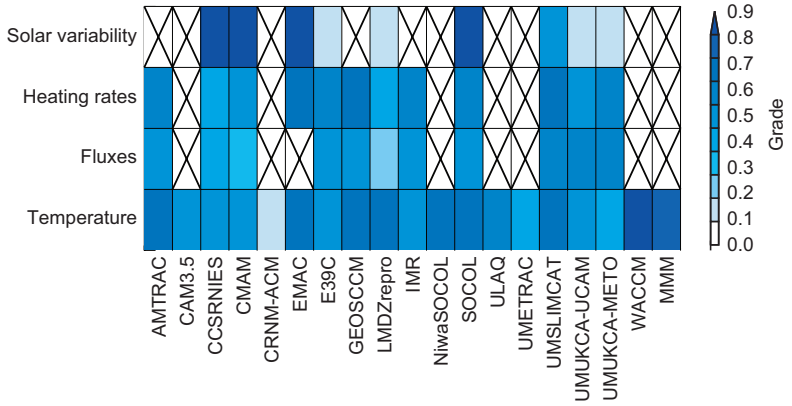

Figure 3.21: A summary of the average CCM grade for temperature related metrics (Figure 3.18), flux related metrics (Figure 3.19), heating rate related metrics (Figure 3.20) and the solar variability metric (see Figure 3.17).

rate changes due to CO_2 are poorly modelled, as are upper stratospheric ozone heating rate changes. The CCM's representation of solar variability is good.

CMAM: This CCM has an adequate representation of climatological global mean temperatures in the lower stratosphere, and a poor representation of temperatures in the middle and upper stratosphere. Global mean temperature trends throughout the stratosphere are well reproduced. Climatological total radiative flux at the tropopause is well modelled. Radiative forcings at the tropopause are well modelled for CH_4 and stratospheric water vapour changes, while stratospheric O_3, CFC, CO_2, N_2O and tropospheric O_3 forcings are poorly modelled. Climatological heating rates and their change from CO_2 and stratospheric O_3 perturbations are either adequate or better. The CCM's representation of solar variability is good.

CNRM-ACM: This CCM has a poor representation of climatological global mean temperatures throughout stratosphere. Global mean temperature trends reproduction in the middle and upper stratosphere are adequate. Reproduction of temperature trends in the lower stratosphere is poor. The CCM's representation of fluxes, heating rates and solar variability is not assessed.

EMAC: This CCM has a good representation of climatological global mean temperatures in the upper stratosphere, adequate representation in the middle stratosphere and poor representation in lower stratosphere. Global mean

temperature trends throughout the stratosphere are well reproduced. Climatological total radiative flux at the tropopause is not assessed. Climatological heating rates are well represented. Changes in heating rates from stratospheric O_3 perturbations are good, expect at upper stratospheric levels where they are adequate. Heating rate changes from CO_2 perturbations are adequate or better, except in the upper stratosphere where they are poor. The CCM's representation of solar variability is good.

E39CA: This CCM has a low model lid so upper stratospheric levels were not assessed. This CCM has an adequate representation of climatological global mean temperatures in the middle stratosphere, and a poor representation of temperatures in the lower stratosphere. Global mean temperature trends throughout the CCM's stratosphere are well reproduced. Climatological total radiative flux at the tropopause is well modelled. Radiative forcings at the tropopause are well modelled for CH_4, CFC, stratospheric O_3 and water vapour changes, both in the stratosphere and troposphere. For CO_2, N_2O and for tropospheric O_3 forcings are poorly modelled. Climatological heating rates and their change from CO_2 and O_3 perturbations are either adequate or better, except in the middle and upper stratosphere for CO_2 changes where representation is poor. The CCM's representation of solar variability is poor.

GEOSCCM: This CCM has a good representation of climatological global mean temperatures throughout the stratosphere. Global mean temperature trends throughout the stratosphere are well reproduced. Climatological total radiative flux at the tropopause is poorly modelled. Radiative forcings at the tropopause are well modelled for water vapour changes, both in the stratosphere and troposphere, and for CH_4, the CFCs, and for tropospheric O_3. Stratospheric O_3 forcing is adequately modelled while CO_2 and N_2O forcings are poorly modelled. Climatological heating rates and their change from CO_2 and stratospheric O_3 perturbations are either adequate or better. The CCM's representation of solar variability is not assessed.

LMDZrepro: This CCM has a good representation of climatological global mean temperatures in the lower and middle stratosphere, and a poor representation of temperatures in the upper stratosphere. Global mean temperature trends throughout the stratosphere are well reproduced. Climatological total radiative flux at the tropopause is poorly modelled. Radiative forcings at the tropopause are well modelled for water vapour changes, both in the stratosphere and troposphere. CH_4 and CFC12 forcings are adequately modelled. CFC11, CO_2, tropospheric O_3 and stratospheric O_3 forcings are all poorly modelled. Climatological heating rates and their change from CO_2 and stratospheric O_3 perturbations are either adequate or better, expect in the middle stratosphere for CO_2 changes and the upper stratosphere for ozone changes where representation is poor. The CCM's representation of solar variability is poor.

MRI: This CCM has a good representation of climatological global mean temperatures in the upper stratosphere, an adequate representation of temperatures in the lower stratosphere, and a poor representation in the middle stratosphere. Global mean temperature trends in the upper and middle stratosphere are well reproduced, whilst temperature trends in the lower stratosphere are adequately reproduced. Climatological total radiative flux at the tropopause is adequately modelled. Radiative forcings at the tropopause are well modelled for water vapour changes in the stratosphere, for O_3 changes both in the stratosphere and troposphere, and for CH_4. CO_2 and water vapour forcings in the troposphere are adequately represented. The forcings from N_2O is poorly represented. CFC forcings are not assessed. Climatological heating rates and their change from CO_2 and stratospheric O_3 perturbations are either adequate or better, expect in the mid- and low stratosphere for CO_2 changes where representation is poor. The CCM's representation of solar variability is not assessed.

NiwaSOCOL: This CCM has a good representation of climatological global mean temperatures in the middle and upper stratosphere and a poor representation in the lower stratosphere. Global mean temperature trends are well reproduced throughout the stratosphere. The CCM's representation of fluxes, heating rates and solar variability is not assessed.

SOCOL: This CCM has a good representation of climatological global mean temperatures in the middle and upper stratosphere and a poor representation in the lower stratosphere. Global mean temperature trends are well reproduced throughout the stratosphere. Climatological total radiative flux at the tropopause is well modelled. Radiative forcings at the tropopause are well modelled for water vapour changes in the stratosphere and troposphere, for O_3 changes in the stratosphere, for CFCs and CH_4. Forcings from CO_2, N_2O, and O_3 changes in the troposphere are poorly represented. Climatological heating rates and their change from CO_2 and stratospheric O_3 perturbations are either adequate or better, expect in the middle and upper stratosphere for CO_2 changes where representation is poor. The CCM's representation of solar variability is good.

ULAQ: This CCM has a good representation of climatological global mean temperatures in the lower and upper stratosphere and an adequate representation in the middle stratosphere. Global mean temperature trends are well reproduced throughout the stratosphere. The CCM's repre-

sentation of fluxes, heating rates and solar variability is not assessed.

UMETRAC: This CCM has a good representation of climatological global mean temperatures in the upper stratosphere, an adequate representation in the middle stratosphere, and a poor representation in the lower stratosphere. Global mean temperature trends are well reproduced in the lower and middle stratosphere and adequately reproduced in the upper stratosphere. The CCM's representation of fluxes, heating rates and solar variability is not assessed.

UMSLIMCAT: This CCM has a good representation of climatological global mean temperatures in the middle and upper stratosphere, and an adequate representation of temperatures in the lower stratosphere. Global mean temperature trends throughout the stratosphere are well reproduced. Climatological total radiative flux at the tropopause is adequately modelled. Radiative forcings at the tropopause are well modelled for ozone changes both in the stratosphere and troposphere, CH_4 and the CFCs. Forcings are adequately modelled for CO_2, N_2O and stratospheric water vapour. Tropospheric water vapour forcing is poorly modelled. Climatological heating rates and their change from CO_2 and stratospheric O_3 perturbations are either adequate or better, expect in the middle stratosphere for CO_2 changes where representation is poor. The CCM's representation of solar variability is adequate.

UMUKCA-METO: This CCM has a good representation of climatological global mean temperatures in the middle and upper stratosphere, and a poor representation of temperatures in the lower stratosphere. Global mean temperature trends in the upper stratosphere are well reproduced, middle stratospheric trends are adequately reproduced and lower stratospheric trends are poorly reproduced. Climatological total radiative flux at the tropopause is well modelled. Radiative forcings at the tropopause are well modelled for stratospheric and tropospheric O_3 changes, N_2O, CFC11 and CH_4. Forcings are adequately modelled for CO_2, CFC12 and stratospheric water vapour. Tropospheric water vapour forcing is poorly modelled. Climatological heating rates and their change from CO_2 and stratospheric O_3 perturbations are either adequate or better, except in the low stratosphere for CO_2 changes where representation is poor. The CCM's representation of solar variability is poor.

UMUKCA-UCAM: This CCM has a good representation of climatological global mean temperatures in the middle and upper stratosphere, and a poor representation of temperatures in the lower stratosphere. Global mean temperature trends throughout the stratosphere are well reproduced. Climatological total radiative flux at the tropopause is well modelled. Radiative forcings at the tropopause are well modelled for tropospheric O_3 change, N_2O, CFC11 and CH_4. Forcings are adequately modelled for CO_2, CFC12, stratospheric O_3 and stratospheric water vapour. Tropospheric water vapour forcing is poorly modelled. Climatological heating rates and their change from CO_2 and stratospheric O_3 perturbations are either adequate or better, expect in the upper stratosphere for O_3 changes and in the low stratosphere for CO_2 changes where representation is poor. The CCM's representation of solar variability is poor.

WACCM: This CCM has a good representation of climatological global mean temperatures throughout the stratosphere. Global mean temperature trends are well reproduced throughout the stratosphere. The CCM's representation of fluxes, heating rates and solar variability is not assessed.

3.6.2 Overall summary

The work in this chapter has shown that CCM global mean temperatures and their change can give an indication of errors in radiative transfer codes and/or atmospheric composition. Biases in the global temperature climatology are generally small, although five out of 18 CCMs shows biases in their climatology that likely indicate problems with their radiative transfer codes. Temperature trends also generally agree well with observations, although one model shows significant discrepancies that appear to be due to radiation errors. Heating rates and estimated temperature changes from CO_2, ozone and water vapour changes are generally well modelled. Other gases (N_2O, CH_4, CFCs) have only played a minor role in stratospheric temperature change but their heating rates are estimated with large fractional errors in many models. Models that do not account for variations in the spectrum of solar irradiance but only consider changes in total (spectrally-integrated) solar irradiance (TSI) cannot properly simulate solar-induced variations in stratospheric temperature. The combined LLGHG global-annual-mean instantaneous net radiative forcing at the tropopause is within 30% of LBL models for all CCM radiation codes tested. Problems remain simulating radiative forcing for stratospheric water vapour and ozone changes with a range of errors between 3% and 200% compared to LBL models.

Performing a comparison of radiation schemes has been challenging. This work would have benefitted from more CCM radiation schemes being run independently of their host models. We suggest that in future radiation schemes should regularly be involved in comparison exercises based on detailed sets of reference calculations from LBL models. Ideally, solar and longwave schemes should be evaluated for a range of realistic circumstances. Future

radiation scheme comparisons should also ideally evaluate the radiative effects of aerosol and cloud as well as trace gases. They should also evaluate the effect of approximations made in CCMs such as the frequency of radiative transfer calculations and the effects of plane-parallel/ sphericity approximations. Photolysis and solar heating calculations should be merged for consistency. Non-local thermodynamic equilibrium effects should be accounted for above 70 km to correctly simulate heating and cooling rates in this region. CCMs should include spectral variations in solar irradiance when modelling solar variability in order to induce the correct stratospheric temperature change. Further work in needed to assess the level of spectral detail required.

References

Austin, J., R. J. Wilson, H. Akiyoshi, S. Bekki, N. Butchart, C. C laud, V. I. Fomichev, P. Forster, R. R. Garcia, N. P. Gillett, P. Keckhut, U. Langematz, E. Manzini, T. Nagashima, W. J. Randel, E. Rozanov, K. Shibata, K. P. Shine, H. Struthers, D. W. J. Thompson, F. Wu, S. Yoden, 2009. Coupled chemistry climate model simulations of stratospheric temperatures and their trends for the recent past. *Geophys. Res. Lett.*, **36**, doi:10.1029/2009GL038462.

Barker, H. W., G. L. Stephens, P. T. Partain, J. W. Bergman, B. Bonnel, K. Campana, E. E. Clothiaux, S. Clough, S. Cusack, J. Delamere, J. Edwards, K. F. Evans, Y. Fouquart, S. Freidenreich, V. Galin, Y. Hou, S. Kato, J. Li, E. Mlawer, J. J. Morcrette, W. O'Hirok, P. Raisanen, V. Ramaswamy, B. Ritter, E. Rozanov, M. Schlesinger, K. Shibata, P. Sporyshev, Z. Sun, M. Wendisch, N. Wood, F. Yang, 2003. Assessing 1D atmospheric solar radiative transfer models: Interpretation and handling of unresolved clouds. *J. Clim.*, **16**, 2676–2699.

Cagnazzo, C., E. Manzini, M. A. Giorgetta, P. M. D. Forster, J. J. Morcrette, 2007. Impact of an improved shortwave radiation scheme in the MAECHAM5 General Circulation Model. *Atmos. Chem. Phys.*, **7**, 2503-2515.

Clough, S.A., and M. J. Iacono, 1995. Line-by-line calculations of atmospheric fluxes and cooling rates. II: Application to carbon dioxide, ozone, methane, nitrous oxide, and the halocarbons. *J. Geophys. Res.*, **100**, 16,519-16,535.

Clough, S. A., M. W. Shephard, E. J. Mlawer, J. S. Delamere, M. J. Iacono, K. Cady-Pereira, S. Boukabara, P. D. Brown, 2005. Atmospheric radiative transfer modeling: a summary of the AER codes, Short Communication, *J. Quant. Spectrosc. Radiat. Transfer*, **91**, 233-244.

Collins, W. D., V. Ramaswamy,, M. D. Schwarzkopf, Y. Sun, R. W. Portmann, Q. Fu, S. E. B. Casanova, J. L. Dufresne, D. W. Fillmore, P. M. D. Forster, V. Y. Galin, L. K. Gohar, W. J. Ingram, D. P. Kratz, M. P. Lefebvre, J. Li, P. Marquet, V. Oinas, Y. Tsushima, T. Uchiyama, W. Y. Zhong, 2006. Radiative forcing by well-mixed greenhouse gases: Estimates from climate models in the Intergovernmental Panel on Climate Change (IPCC) Fourth Assessment Report (AR4). *J. Geophys. Res.*, **111**, doi:10.1029/2005JD006713.

Egorova, T., E. Rozanov, E. Manzini, M. Haberreiter, W. Schmutz, V. Zubov, and T. Peter, 2004. Chemical and dynamical response to the 11-year variability of the solar irradiance simulated with a chemistry-climate model, *Geophys. Res. Lett.*, **31**, doi:10.1029/2003GL019294.

Ellingson, R. G., S. J. Ellis,, S. B. Fels, 1991. The intercomparison of radiation codes used in climate models - Long-wave results, *J. Geophys. Res.*, **96**, 8929–8953.

Feigelson, E. M., and L. R. Dmitrieva (eds.), 1983. Radiative algorithms in the atmospheric general circulation models: A review, Inf. VNIGMI-MCD, issue 1, Obninsk.

Fomichev, V. I., 2009. The radiative energy budget of the middle atmosphere and its parameterizations in general circulation models. *J. Atmos. Solar-Terr. Phys.*, **71**, 1577-1585.

Fomichev, V. I., J.-P. Blanchet, D. S. Turner, 1998. Matrix parameterization of the 15 μm CO2 band cooling in the middle and upper atmosphere for variable CO2 concentration. *J. Geophys. Res.*, **103**, 11505 - 11528.

Fomichev, V. I., C. Fu, J. de Grandpré, S. R. Beagley, V. P. Ogibalov, J. C. McConnell, 2004. Model thermal response to minor radiative energy sources and sinks in the middle atmosphere. *J. Geophys. Res.*, **109**, doi:10.1029/2004JD004892.

Fomin, B.A., 2006. Monte-Carlo algorithm for line-by-line calculations of thermal radiation in multiple scattering layered atmospheres. *J. Quant. Spectrosc. Rad.*

Transfer, **98**, 107-115.

Fomin, B.A., and I. P. Mazin, 1998. Model for an investigation of radiative transfer in cloudy atmosphere. *Atmospheric Research*, **48**, 127-153.

Forster, P. M. D., M. Ponater, W. Y. Zhong, 2001. Testing broadband radiation schemes for their ability to calculate the radiative forcing and temperature response to stratospheric water vapour and ozone changes. *Meteorol. Z.*, **10**, 387-393.

Forster, P., V. Ramaswamy, P. Artaxo, T. Berntsen, R. Betts, D.W. Fahey, J. Haywood, J. Lean, D.C. Lowe, G. Myhre, J. Nganga, R. Prinn, G. Raga, M. Schulz, R. Van Dorland, 2007. Changes in Atmospheric Constituents and in Radiative Forcing. In: Climate Change 2007: The Physical Science Basis. Contribution of Working Group I to the Fourth Assessment Report of the Intergovernmental Panel on Climate Change. Cambridge University Press, Cambridge, United Kingdom and New York, NY, USA.

Fouquart, Y., B. Bonnel, V. Ramaswamy, 1991. Intercomparing shortwave radiation codes for climate studies, *J. Geophys. Res.*, **96**, 8955–8968.

Goldblatt, C., T. M. Lenton, A. J. Watson, 2009. An evaluation of the long-wave radiative transfer code used in the Met Office Unified Model. *Quart. J. Roy. Meteorol., Soc.*, **135**, 619-633.

Haigh, J. D., 1994. The role of stratospheric ozone in modulating the solar radiative forcing of climate. *Nature*, **370**, 544-546.

Halthore, R. N., D. Crisp, S. E. Schwartz, G. P. Anderson, A. Berk, B. Bonnel, O. Boucher, F. L. Chang, M. D. Chou, E. E. Clothiaux, P. Dubuisson, B. Fomin, Y. Fouquart, S. Freidenreich, C. Gautier, S. Kato, I. Laszlo, Z. Li, J. H. Mather, A. Plana-Fattori, V. Ramaswamy, P. Ricchiazzi, Y. Shiren, A. Trishchenko, W. Wiscombe, 2005. Intercomparison of shortwave radiative transfer codes and measurements. *J. Geophys. Res.*, **110**, doi:10.1029/2004JD005293.

Jonsson, A. I., V. I. Fomichev, T. G. Shepherd, 2009. The effect of nonlinearity in CO2 heating rates on the attribution of stratospheric ozone and temperature changes, *Atmos. Chem. Phys.*, **9**, 8447-8452.

Kiehl, J. T., C. Bruhl, T. Yamanouchi, 1985. A parameterization for the absorption due to the near infrared bands of CO2. *Tellus*, **37B**, 189-196.

Lacis, A. A., and J.E. Hansen, 1974. A parameterization for the absorption of solar radiation in the Earth's atmosphere. *J. Atmos. Sci.*, **31**, 118-133.

Lean, J. L., G. Rottman, J. Harder, G Kopp, 2005. SORCE contributions to new understanding of global change and solar variability. *Solar Phys.*, **230**, 27-53.

Li, J., and H. W. Barker, 2005. A radiation algorithm with correlated-k distribution. Part I: Local thermal equilibrium. *J. Atmos. Sci.*, **62**, 286-309.

Luther, F. M., R.G. Ellingson, Y. Fouquart, S. Fels, N. A. Scott, W. J. Wiscombe, 1988. Intercomparison of radiation codes in climate models (ICRCCM) - Longwave clear-sky results - A workshop summary. *Bull. Am. Meteorol. Soc.*, **69**, 40-48.

Mayer, B., and A. Kylling, 2005. Technical Note: The LibRadtran software package for radiative transfer calculations: Description and examples of use. *Atmos. Chem. Phys.*, **5**, 1855–1877.

Myhre, G., and F. Stordal., 1997. Role of spatial and temporal variations in the computation of radiative forcing and GWP. *J. Geophys. Res.*, **102**, 11181–11200.

Myhre, G., and F. Stordal, 2001. On the tradeoff of the thermal and solar radiative impact of contrails. *Geophys. Res. Lett.*, **28**, 3119–3122.

Myhre, G., F. Stordal, I. Gausemel, C. Nielsen, and E. Mahieu, 2006. Line-by-line calculations of thermal infrared radiation representative for global condition: CFC-12 as an example. *J. Quant. Spec. Rad. Trans.*, **97**, 317-331.

Myhre, G., M. Kvalevåg, G. Rädel, J. Cook, K. P. Shine, H. Clark, F. Karcher, K. Markowicz, A. Kardas, P. Wolkenberg, Y. Balkanski, M. Ponater, P. Forster, A. Rap, R. R. de Leon, 2009. Intercomparison of radiative forcing of stratospheric water vapour and contrails. *Meteorol. Z.*, **18**, 585-596.

Nissen, K., K. Matthes, U. Langematz, B. Mayer, 2007. Towards a better representation of the solar cycle in general circulation models. *Atmos. Chem. Phys.*, **7**, 5391-5400.

Ogibalov, V. P., and V. I. Fomichev, 2003. Parameterization of solar heating by the near IR CO2 bands in the mesosphere. *Adv. Space Res.*, **32**, 759-764.

Portmann, R., S. Solomon, J. Fishman, J. Olson, J. Kiehl, B. Briegleb, 1997. Radiative forcing of the Earth's climate system due to tropical tropospheric ozone production, *J. Geophys. Res.*, **102**, 9409-941.

Randel, W. J., and F. Wu, 2007. A stratospheric ozone profile data set for 1979–2005: Variability, trends, and comparisons with column ozone data. *J. Geophys. Res.*, **112**, doi:10.1029/2006JD007339

Randel, W. J., K. P. Shine, J. Austin, J. Barnett, C. Claud,

N. P. Gillett, P. Keckhut, U. Langematz, R. Lin, C. Long, C. Mears, A. Miller, J. Nash, D. J. Seidel, D. W. J. Thompson, F. Wu, S. Yoden, 2009. An update of observed stratospheric temperature trends. *J. Geophys. Res.*, **114**, doi:10.1029/2008JD010421.

Shine, K. P., M. S. Bourqui, P. M. Forster, S. H. E. Hare, U. Langematz, P. Braesicke, V. Grewe, M. Ponater, C. Schnadt, C.A. Smiths, J. D. Haigh, J. Austin, N. Butchart, D. T. Shindell, W. J. Randel, T. Nagashima, R. W. Portmann, S. Solomon, D. J. Seidel, J. Lanzante, S. Klein, V. Ramaswamy, M. D. Schwarzkopf, 2003. A comparison of model-simulated trends in stratospheric temperatures. *Quart. J. Roy. Meteor. Soc.*, **129**, 1565–1588.

Taylor, K. E., 2001. Summarizing multiple aspects of model performance in a single diagram. *J. Geophys. Res.*, **106**, 7183-7192.

WMO, 2003. Scientific assessment of ozone depletion: 2002. Tech. Rep. 47, Global Ozone Research and Monitoring Project, World Meteorological Organization, Geneva, Switzerland, 498 pp.

World Meteorological Organization (WMO)/United Nations Environment Programme (UNEP), 2007. *Scientific Assessment of Ozone Depletion: 2006*, World Meteorological Organization, Global Ozone Research and Monitoring Project, Report No. 50, Geneva, Switzerland.